Michael Franz KRENN, BSc

Spin-Peierls Transitions of 1D and 2D Spin-1/2 Heisenberg Models based on Quantum Monte-Carlo Simulations in Interaction Representation

MASTERARBEIT

zur Erlangung des akademischen Grades
Diplom-Ingenieur

Masterstudium Technische Physik

Institut für Theoretische Physik - Computational Physics
Technische Universität Graz

Betreuer:
Ao.Univ.-Prof. Dipl.-Phys. Dr.rer.nat. Hans Gerd Evertz

Graz, Mai 2011

Deutsche Fassung:
Beschluss der Curricula-Kommission für Bachelor-, Master- und Diplomstudien vom 10.11.2008
Genehmigung des Senates am 1.12.2008

EIDESSTATTLICHE ERKLÄRUNG

Ich erkläre an Eides statt, dass ich die vorliegende Arbeit selbstständig verfasst, andere als die angegebenen Quellen/Hilfsmittel nicht benutzt, und die den benutzten Quellen wörtlich und inhaltlich entnommene Stellen als solche kenntlich gemacht habe.

Graz, am ……. ……..
(Unterschrift)

Englische Fassung:

STATUTORY DECLARATION

I declare that I have authored this thesis independently, that I have not used other than the declared sources / resources, and that I have explicitly marked all material which has been quoted either literally or by content from the used sources.

……. ……..
date (signature)

Abstract

In this thesis we primarily study the one- and two-dimensional spin-1/2 Heisenberg model coupled to phonons, both static (classic lattice displacement) and dynamic (quantum mechanical description of lattice degrees of freedom). Lattice degrees of freedom acting on spins can cause a structural quantum phase transition from uniform to dimerized phase, the so called Spin-Peierls Transition (SPT). Such a structural transition can be experimentally observed in materials like the quasi one-dimensional Bechgaard-salt.

The different models with phonons are investigated by Quantum Monte-Carlo (QMC) simulations, treating the partition function in a Stochastic Series Expansion (SSE). The lattice degrees of freedom are introduced in the so called interaction representation. A Fast Fourier Transform, which costs most of the computational effort, transforms the configurations to momentum and frequency space in which new phonon configurations can be sampled efficiently. The spins are updated via a directed loop algorithm. Via this algorithms site and bond phonons and any bare phonon dispersion can be implemented. This thesis is restricted to discussions of dispersion-less optical phonons. A mapping between SSE and continuous imaginary time is used for an efficient calculation of spectra of spin excitations. Since simulations with large spin-phonon couplings suffer from large autocorrelation, a tempering technique in terms of the phonon coupling constant, was implemented.

Based on work by J. Sirker for static phonon interactions we study the ferromagnetic Heisenberg model in one dimension which has a phase transition at finite temperature.
In one dimension, the Mermin-Wagner theorem states that a phase transition can only take place at $T = 0$. In the antiferromagnetic chain such a transition takes place at finite spin-phonon coupling. Although a Mean Field calculation indicates a transition, QMC calculations verify that no dimerization occurs in the phonon coordinates.

We then investigate two-dimensional systems of coupled chains. To reduce computational effort the phonons are only introduced along the chains. For static phonons and ferromagnetic spin coupling we calculate the spin spectra by QMC and determine the spin energy as a function of phonon displacement at different temperatures. Similar to the one-dimensional case we find an energy gain at large T.
From work by F. Michel it is known that there is a zero-temperature phase transition with dynamic phonons for AF coupling. We investigate the FM case and estimate the critical coupling in a Mean Field calculation.
Finally we perform QMC calculations with dynamic phonons, which turns out to suffer from large autocorrelations at large phonon coupling. Nonetheless they show a very strong indication that there is indeed a phase transition to a dimerized phase for the two-dimensional FM Heisenberg model at finite temperature.

Results for the spin-1-Heisenberg model, the anisotropic Heisenberg model and 'free fermions' are shown in the appendices.

Kurzfassung

In dieser Arbeit wird primär das Spin-1/2 Heisenberg Modell einerseits mit statischer (klassischer Betrachtung der Auslenkung) und andererseits mit dynamischer (quantenmechanischer Beschreibung der Freiheitsgrade der Gitterschwingung) Phononenkopplung untersucht. Die auf die Spins wirkenden Freiheitsgrade der Gitterschwingung können einen strukturellen Quantenphasenübergang von einer uniformen zu einer dimerisierten Phase, den sogenannten Spin-Peierls Übergang verursachen. Ein derartiger struktureller Übergang kann für Materialien ähnlich dem quasi eindimensionalen Bechgaard-Salz experimentell gemessen werden.

Die verschiedenen Modelle werden mittels Quanten Monte-Carlo (QMC) Simulationen unter der Verwendung der stochastischen Reihenentwicklung (Stochastic Series Expansion SSE) der Zustandssumme untersucht. Die Freiheitsgrade der Gitterschwingung werden in der sogenannten Wechselwirkungsdarstellung implementiert. Eine Fourier Transformation, die einen erheblichen Anteil des Rechenaufwands benötigt, transformiert die Konfiguration in den Impuls- und Frequenzraum, in dem die neuen Phononenkonfigurationen effizient gezogen werden können. Die Aktualisierung der Spins erfolgt mit dem 'direct loop' Algorithmus. Unter Verwendung dieser Algorithmen können die 'site' und 'bond' Phononen und alle 'nackten' Phononen realisiert werden, wobei diese Arbeit auf die Untersuchung der dispersionslosen optischen Phononen eingeschränkt ist. Eine Abbildung zwischen der SSE und der kontinuierlich imaginären Zeitdarstellung wird für eine effiziente Berechung der Spektren der Spin-Anregungen gewählt. Da gerade Simulationen mit großer Spin-Phononenkopplung starker Autokorrelationen unterliegen wird ein 'Tempering' bezüglich der Kopplung durchgeführt.

Basierend auf der Arbeit von J. Sirker für statische Phononenwechselwirkung untersuchen wir das eindimensionale, ferromagnetische Heisenberg Modell, welches in endlicher Temperatur einen Phasenübergang aufzeigt. Das Mermin-Wagner Theorem besagt ein Auftreten eines Phasenübergangs in ei-

ner Dimension lediglich bei $T = 0$.
Für antiferromagnetische Ketten tritt ein derartiger Übergang bei endlicher Spin-Phononenkopplung auf. Obwohl im Zuge einer 'Mean Field' Näherung das Auftreten eines Überganges aufgezeigt wird, ergeben die QMC Berechungen keine auftretende Dimerisierung für die Phononen-Koordinaten.

Anschließend untersuchen wir zweidimensionale Systeme von gekoppelten Ketten. Um den rechentechnischen Aufwand zu reduzieren werden die Phononen nur entlang der Ketten implementiert. Für statische Phononen und ferromagnetische Spinkopplung werden Spin-Spektren berechnet und die Spinenergie als Funktion der Auslenkung für unterschiedliche Temperaturen ermittelt. Analog zum eindimensionalen Fall tritt ein Energiegewinn bei hohen Temperaturen auf.
Nach der Arbeit von F. Michel ist ein Phasenübergang mit dynamischen Phononen und AF Kopplung für die Temperatur Null bekannt. Wir untersuchen den FM Kopplungsfall und ermitteln mittels 'Mean Field' Berechungen die kritische Kopplung.
Abschließend führen wir QMC Berechungen mit dynamischen Phononen aus, die - wie sich herausstellt - bei großen Phononenkopplungen großer Autokorrelationen unterliegen. Trotz alledem zeigen diese Berechungen sehr starke Anzeichen eines Phasenübergangs in eine dimerisierte Phase für das zweidimensionale FM Heisenberg Modell mit endlichen Temperaturen an.

In den Anhängen sind Resultate für das Spin-1 Heisenberg Modell, das anisotrope Heisenberg Modell und für freie Fermionen enthalten.

Contents

Chapter 1

Introduction

In modern solid state physics strongly correlated particle systems are one of the most investigated objects. New electrical and magnetical effects like the high temperature superconductor and the prospect of new technologies are reasons for enormous effort in research on strongly correlated electron systems. Even simple models, like the spin-1/2 Heisenberg model, are keys in describing magnetic properties of such compounds. Inserting lattice degrees of freedom in this correlated system, calculating magneto-elastic properties and quantum phase transitions, will be the topic of this thesis.

1.1 Spin-Peierls Transition

The Spin-Peierls Transition is a structural phase transition caused by the interaction of spins and phonons, where magnetic energy is gained by distorting the lattice, first found by Rudolf Peierls [1] in 1955 for one-dimensional metals. It is found that this system is unstable under a lattice deformation with wave vectors twice the Fermi wave vector ($2\mathbf{k}_F$).
For this spin system it is energetically favorable to compensate the lattice deformation in a symmetry breaking, shown in the energy vs. phonon displacement behavior Fig. 1.1 and with an energy gap in the dispersion relation.
In recent years the Spin-Peierls Transition has been investigated in the antiferromagnetic Heisenberg model (see in one dimension Sec. 5.1 and in two dimensions Sec. 7.1 and e.g. Michel et al. [2], [3]). In this thesis we now want to query whether there is a Spin-Peierls transition in the ferromagnetic case for one- (see Sec. 5.2, determined by Sirker et. al [4] by classical treatment of the lattice) or two-dimensional Heisenberg models (see Sec. 7.2).

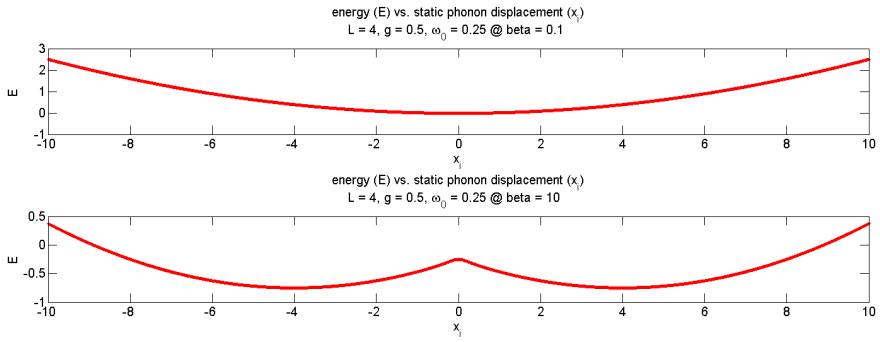

Figure 1.1: Symmetry breaking of a static phonon displaced one-dimensional Heisenberg model. The minimum of the energy, related to the static phonon displacement x_i at $x_i = 0$, splits up into two by lowering the temperature, here shown in an exact diagonalization calculation (more about this in Chapter 4)

Chapter 2

Hamiltonian

2.1 Chains

The Heisenberg model is a simple, but effective model to describe magnetic properties of materials, like critical points and phase transitions. If weak interactions between electrons are neglected, effects of complex structures can be calculated by a remaining one-dimensional spin-spin interaction. This is the one-dimensional antiferromagnetic Heisenberg model. In Fig. 2.1 we can see such a complex structure, the 'quasi-one-dimensional Bechgaard salt'.

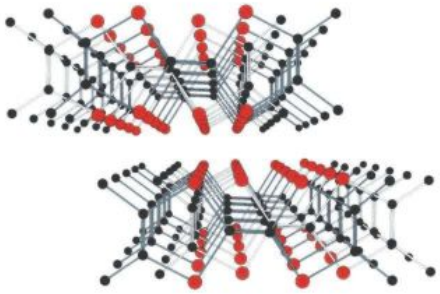

Figure 2.1: Quasi-one-dimensional Bechgaard salt, taken from [5]

The well known one-dimensional Hamiltonian with next nearest neighbor interaction is described by:

$$\hat{H} = \sum_{i=1}^{N} J_z \; S_i^z S_{i+1}^z + J_{xy} \left(S_i^x S_{i+1}^x + S_i^y S_{i+1}^y \right) \tag{2.1}$$

where J_z and J_{xy} are the exchange constants in $z-$ or planar $xy-$direction respectively, N is the number of spins and $\mathbf{S}_i$ is the spin-1/2 operator acting on site i. The planar xy-component of the Hamiltonian is rewritten by ladder operators:

$$S_i^x S_{i+1}^x + S_i^y S_{i+1}^y = \frac{1}{2}\left(S_i^+ S_{i+1}^- + S_i^- S_{i+1}^+\right) \tag{2.2}$$

This leads to the resulting Hamiltonian:

$$\hat{H} = \sum_{i=1}^{N} J_z \; S_i^z S_{i+1}^z + \frac{J_{xy}}{2}\left(S_i^+ S_{i+1}^- + S_i^- S_{i+1}^+\right) \tag{2.3}$$

In Fig. 2.2 we can give a brief overview of the different models of the one-dimensional Hamiltonian. If $J_z = J_{xy} = J$ we get the isotropic Heisenberg model, the ferromagnetic case at $J = -1$ and the antiferromagnetic one at $J = 1$. Doing the limit $\frac{J_z}{J_{xy}} \to \infty$ or $\frac{J_z}{J_{xy}} \to -\infty$ leads to the antiferromagnetic or ferromagnetic Ising model. Setting the exchange constant in z-direction to zero ($J_z = 0$) results to the xy-model. Apart from the above-mentioned models the Hamiltonian is called anisotropic Heisenberg model.

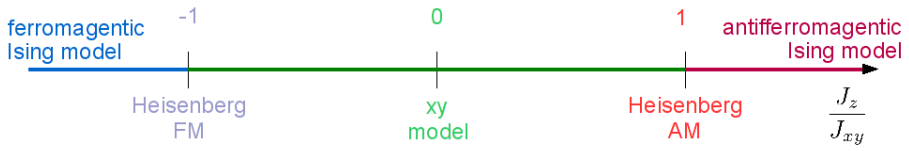

Figure 2.2: Different regimes of the one-dimensional Hamiltonian

Although the Heisenberg model seems to be a simple model, an analytic solution only exists for the one-dimensional spin-1/2 case, using the so called Bethe ansatz [6]. Not only the ground state, but also excited states [7] and the thermodynamics of this model based on the Bethe ansatz solution to the quantum transfer matrix [8] can be calculated in a numerically exact way.
The Mermin-Wager theorem [9] says that a phase transition at finite temperature will not occur in the one-dimensional Heisenberg model, therefore in one dimension no long range order can be seen.
The spin-spin correlation behaves like:

$$\langle \mathbf{S}_i \mathbf{S}_j \rangle \propto \frac{1}{|i-j|} \tag{2.4}$$

In Appendices B and C we do some anisotropic Heisenberg ($J_z = \frac{1}{2}J_{xy}$) and 'free fermions' ($J_{xy} \neq J_z = 0$) calculations.

2.2 Chains with static phonon interaction

Couplings between spins and lattice vibrations (phonons) can provoke structural instabilities. In a simple manner, a classical treatment of the lattice is realized in the Heisenberg model by implementing a static phonon interaction $f(i)$, Eq. (2.6), see Fig. 2.3.

$$\hat{H} = \sum_{i=1}^{N} f(i) \left\{ J_z \; S_i^z S_{i+1}^z + \frac{J_{xy}}{2} \left(S_i^+ S_{i+1}^- + S_i^- S_{i+1}^+ \right) \right\} \tag{2.5}$$

The static phonon interaction is a periodically[1] alternating change of the spin-spin interaction with respect to the site index i. Its strength is specified by the dimensionless parameter $\delta = 2gu/(|J|a_0)$, given by g the spin-phonon coupling constant, a_0 the lattice constant, u the atomic displacement and J the exchange constant[2], shown in the paper of Sirker et al. [4].

$$f(i) = 1 + (-1)^i \delta \tag{2.6}$$

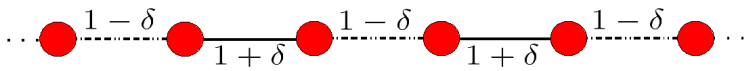

Figure 2.3: Heisenberg model with static phonon interaction $J \cdot (1 \pm \delta)$

The lattice displacements are concerned by an additional elastic energy:

$$E_{el} = \frac{NK\delta^2}{2} \tag{2.7}$$

which yields the total adiabatic approximated Hamiltonian, where $K = \tilde{K}J^2a_0^2/(4g^2)$ is the effective elastic constant and $\tilde{K}$ determines the energy of N coupled harmonic oscillators $E_{el} = N\tilde{K}u^2/2$. A Spin-Peierls transition occurs when the gain in magnetic energy is larger than the loss in elastic energy. This is discussed in Chap. 4.

[1] $f(i+k) = f(i);\ k \in \{p \bmod N \equiv 0\},\ p \in N$
[2] $J = J_z = J_{xy}$

2.3 Chains with dynamic phonon interaction

To specify the dynamic phonon interaction, we insert a spin-phonon coupling function $f(x_i)$, which is based on the phonon displacement x_i at a specific site i, and add H_p the Hamiltonian of the non-interacting phonons, in the one-dimensional Heisenberg model.

$$\hat{H} = \sum_{i=1}^{N} f(x_i) \left\{ J_z \; S_i^z S_{i+1}^z + \frac{J_{xy}}{2} \left(S_i^+ S_{i+1}^- + S_i^- S_{i+1}^+ \right) \right\} + H_p \tag{2.8}$$

Two different kinds of phonons are often considered. The first one consists of bond phonons Eq. (2.9), where ions between spins oscillate perpendicularly to the spin chain (transverse oscillation). The positions of the spins do not change, but the exchange coupling is modified. The strength of the interaction between spins and phonons is specified by the coupling constant g. Setting it to zero it gives us back the 'simple' Heisenberg model, apart from H_p.

$$f(x_i) = 1 + g \cdot x_i \tag{2.9}$$

The second type consists of longitudinal oscillations of the ions along the chain, so called site phonons. This is shown in Eq. (2.10), containing differences of the phonon displacements of the next nearest neighbor sites.

$$f(x_i) = 1 + g \cdot (x_i - x_{i-1}) \tag{2.10}$$

The non-interacting Hamiltonian H_p can be specified in Fourier space, where q is the reciprocal lattice point of the first Brillouin-Zone and $\omega(q)$ gives the bare phonon dispersion.

$$H_p = \sum_{q}^{1B.Z.} \frac{p_q^2}{2} + \frac{\omega^2(q)}{2} x_q^2 \tag{2.11}$$

We consider two archetypal kinds of bare phonon dispersions $\omega(q)$. When the phonons couple like $(x_i - x_{i+1})^2$ in H_{ph} then the dispersion in $\omega-$space, obtained by a Fourier transform, is Eq. (2.12).

$$\omega(q) = \frac{\omega_0}{\sqrt{2}} \sqrt{1 - \cos(q)} \tag{2.12}$$

These are gap-less acoustic phonons, shown in Fig. 2.4.
Optical phonons based on the Fourier transform of x_i^2 are described by dispersion-less Einstein phonons, shown below 2.13 and in Fig. 2.4.

$$\omega(q) = \omega_0 \tag{2.13}$$

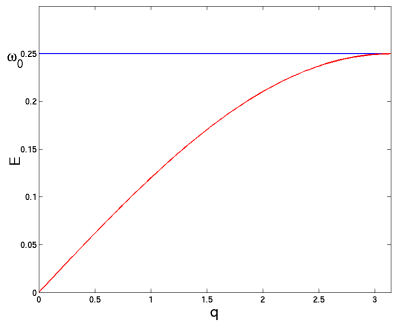

Figure 2.4: The dispersion-less Einstein phonons approximate the optical branch (blue) and the gap-less acoustic phonons form an acoustic branch (red) [10]

2.4 Square lattice

The arrangement of the spins of the one-dimensional Heisenberg model (Heisenberg chain) exemplified above is expanded to an additional dimension. The spins in the second dimension are coupled via a perpendicular exchange-coupling constant $J_\perp$. This yields the two-dimensional Heisenberg model:

$$\hat{H} = J_\parallel \sum_{i,j=1}^{N} \mathbf{S}_{i,j}\mathbf{S}_{i+1,j} + J_\perp \sum_{i,j=1}^{N} \mathbf{S}_{i,j}\mathbf{S}_{i,j+1} \tag{2.14}$$

One material which can be described by the two-dimensional Heisenberg model is $SrCu_2(BO_3)_2$. The structure is shown in Fig. 2.5.

For the two-dimensional case with larger system size no exact solution is available and a numerical treatment is needed. As the Mermin-Wagner theorem [9] states, no phase transition can be observed at finite temperature. The spin correlation $\langle \mathbf{S}_i \mathbf{S}_j \rangle$ shows an exponential decreasing behavior within the distance $|i - j|$, see Ding et al. [12].

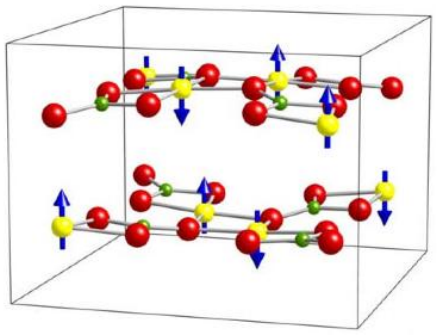

Figure 2.5: $SrCu_2(BO_3)_2$ describable by a two-dimensional antiferromagnetic Heisenberg model, taken from [11]

2.5 Square lattice with static phonon interaction in one dimension

There are different ways static phonon displacements can occur in a two-dimensional Heisenberg model (see Sirker et al. [13] and Wenzel et al. [14]). The weaker[3] and stronger[4] spin couplings can be either placed in a zig-zag string in the lattice or in a periodically alternating coupling of fixed chains. Treating the latter case, the coupling constant $J_\perp$ is shown in Fig. 2.6, with $f(i)$ of Eq. (2.15), which is applied in this thesis.

$$\hat{H} = J_\parallel \sum_{i,j=1}^{N} f(i) \{\mathbf{S}_{i,j}\mathbf{S}_{i+1,j}\} + J_\perp \sum_{i,j=1}^{N} \mathbf{S}_{i,j}\mathbf{S}_{i,j+1},$$
$$f(i) = 1 + (-1)^i \delta \tag{2.15}$$

In order to study the Spin-Peierls Transition (SPT) as already discussed in Sec. 2.2, we have to take care of the elastic energy E_{el}. In Chap. 6 we once more calculate a possible gain in magnetic energy versus cost in elastic energy.

[3] $J_\parallel(1-\delta)$
[4] $J_\parallel(1+\delta)$

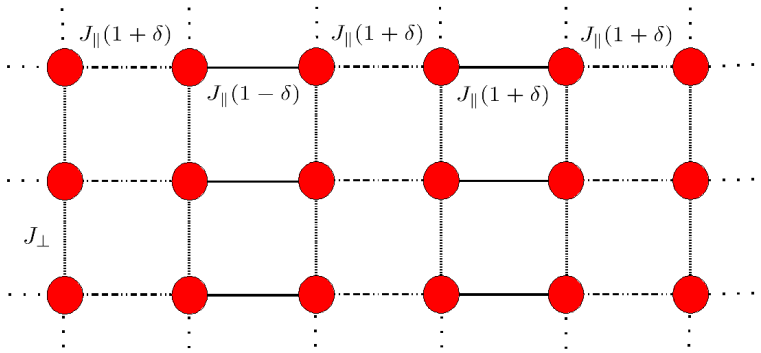

Figure 2.6: Heisenberg model with static phonon interaction in one dimension $J_\parallel(1 \pm \delta)$ and coupling constant $J_\perp$ in second dimension

2.6 Square lattice with dynamic phonon interaction in one dimension

The dynamic phonon interaction Eqs. (2.16) and (2.11) is just[5] applied in one dimension[6]. The second dimension is coupled with a exchange coupling constant $J_\perp$, therefore the model describes coupled Heisenberg chains.

$$\hat{H} = J_\parallel \sum_{i,j=1}^{N} f(x_i) \{\mathbf{S}_{i,j}\mathbf{S}_{i+1,j}\} + J_\perp \sum_{i,j=1}^{N} \mathbf{S}_{i,j}\mathbf{S}_{i,j+1} + H_p,$$
$$f(x_i) = 1 + g \cdot (x_i - x_{i-1}) \tag{2.16}$$

[5]because of computational effort, we will see in Sec. 3.5 and D

[6]Plotting the dispersion we will get a single phonon branch, instead of usually two - we may expect in a two-dimensional lattice.

Chapter 3

Quantum Monte-Carlo

3.1 Introduction to Quantum Monte-Carlo

When dealing with large system sizes, numerical methods - like the Quantum Monte-Carlo - are essential instruments for understanding physical effects, especially in condensed matter physics[1]. In this thesis we are dealing with high dimensional integrals, low temperatures and especially with dynamical effects like the dynamical phonon interaction. Therefore improvements of QMC algorithms, their efficiency and possible usage are continuously under development.

In the past, the Trotter-Suzuki decomposition formula (see Suzuki et al. [16] and Trotter et al. [17]) was used to formulate a Euclidean time path integral (partition function) ready for finite-temperature Quantum Monte-Carlo simulation. The inverse temperature is treated as an imaginary time evolution[2]. By discretization of this imaginary time $\Delta\tau$ a systematic error appears, scaled as $(\Delta\tau)^2$. Handling this systematic error, measurements have to be extrapolated by doing several simulations with different $\Delta\tau$, which costs a lot of computational effort. More recently, it has been become clear that one can take the time continuum limit in this formulation and perform once directly in this limit (see Evertz [18]).
Alternately, the systematic error vanishes by treating the path integral with the Stochastic Series Expansion (SSE), Sandvik et al. [19], introducing the space of operator sequences. This approach is taken in this thesis.
On the other hand, the advantage of the Trotter-Suzuki decomposition and

[1] Because of the enormous Hilbert space the Lanczos algorithm [15] is not suitable anymore.

[2] The Quantum-MC is projected to classical Monte-Carlo by inserting the imaginary time as an additional dimension.

its usage of imaginary time is the comfortable implementation of Green's function calculations, whereas in the SSE formulation, Green's functions are very cumbersome to calculate. This problem can be solved by a mapping between SSE operator string index and continuous time (Michel [2]).
For the spin-phonon interaction, the spin update is done by using the directed loop algorithm, with constant phonon coordinates. Phonon updates are performed for fixed spins, in a time-state process. A modified bilinear interaction is used to propose a global new phonon configuration, which is than accepted or rejected using the actual interaction, see Michel [2].

3.2 Stochastic Series Expansion (SSE)

We want to get a basic overview of the Stochastic Series Expansion (SSE)[3], see more about in Sandvik et al. [19] [21] and Evertz [18]. We start our derivation with the thermodynamic expectation value for an operator $\hat{A}$ at a certain inverse temperature β.

$$\langle \hat{A} \rangle = \frac{1}{Z} \mathrm{Tr} \left\{ \hat{A} e^{-\beta \hat{H}} \right\}, \tag{3.1}$$

$$Z = \mathrm{Tr}\ e^{-\beta \hat{H}} \tag{3.2}$$

The exponential operator is Taylor expanded and the trace of the partition function Z is written in a specific basis $|\alpha\rangle$. For the Heisenberg model Eq. (2.3) the $|\alpha\rangle = |S_1^z, S_2^z, ..., S_N^z\rangle$ basis is chosen.

$$Z = \sum_{\alpha} \sum_{n=0}^{\infty} \frac{\beta^n}{n!} \langle \alpha | \left(-\hat{H}\right)^n | \alpha \rangle \tag{3.3}$$

By rewriting the Hamiltonian as a sum of diagonal and off-diagonal operators[4], acting on each bond b_i, the SSE configuration space is spanned.

$$\hat{H} = -\sum_{i=1}^{n} \hat{h}_{a_i, b_i} \tag{3.4}$$

In case of the Heisenberg model the diagonal operator $\hat{h}_{1,b_i}$ is $J_z(S_{b_i}^z S_{b_j}^z + C)$, with b_i the bond index of next nearest neighbors $\langle i, j \rangle$. A constant C is

[3] Our simulations are based on the implementation of the '**A**lgorithms and **L**ibraries for **P**hysics **S**imulations' packages [20].

[4] $a_i = 1$: diagonal operator; $a_i = 2$: off-diagonal operator;

added to guarantee the positivity of the matrix elements (see Evertz [18]). The off-diagonal operator $\hat{h}_{2,b_i}$ is described by $J_{xy}(S^+_{b_i}S^-_{b_j} + S^-_{b_i}S^+_{b_j})$.
Under periodic boundary conditions, the propagation of the states is now written in the following way Eq. (3.5).

$$\begin{aligned} |\alpha(p)\rangle &= \prod_{i=1}^{p} \hat{h}_{a_i,b_i} |\alpha(0)\rangle \,, \\ |\alpha(\tilde{L})\rangle &= |\alpha(0)\rangle \end{aligned} \tag{3.5}$$

Back to the expansion formulation we can describe the n^{th} power of the Hamiltonian as a product of operators:

$$(-\hat{H})^n = \underbrace{(\hat{h}_{a_1,b_1} + \hat{h}_{a_2,b_2} + ...)(\hat{h}_{a_1,b_1} + \hat{h}_{a_2,b_2} + ...)...(\hat{h}_{a_1,b_1} + \hat{h}_{a_2,b_2} + ...)}_{\text{n-times}} \tag{3.6}$$

The expansion is truncated at some $n \sim N\beta$, which leads to a vanishing exponential contribution, but not to a systematic error[5]. Implementing unitary operators $h_{0,0} = \hat{\mathbb{1}}$ in the sequence leads to a fixed operator sequence length $\tilde{L}$.

$$(-\hat{H})^n = \sum_{\substack{\text{sequences } S_n \\ S_n \in \left\{(a_1,b_1)_1,\ldots,(a_{\tilde{L}},b_{\tilde{L}})_{\tilde{L}}\right\}}} \underbrace{\hat{h}_{a_1,b_1}\hat{h}_{a_2,b_2}...\hat{h}_{a_n,b_n}\hat{\mathbb{1}}\hat{\mathbb{1}}\hat{\mathbb{1}}}_{\tilde{\text{L}} \text{ - times}} \tag{3.7}$$

The partition function is shown beneath, the number of ways introducing $(\tilde{L} - n)$ unitary operators is compensated by the prefactor:

$$Z = \sum_{\alpha} \sum_{n=0}^{\tilde{L}} \sum_{S_n} \frac{\beta^n (\tilde{L} - n)!}{\tilde{L}!} \langle\alpha| \prod_{i=1}^{\tilde{L}} \hat{h}_{a_i,b_i} |\alpha\rangle = \sum_{\alpha} \sum_{n=0}^{\tilde{L}} \sum_{S_n} W(\alpha, S_n) \tag{3.8}$$

[5]Brainstorming: As during the simulation the upper limit of the configuration space will not be reached (there are still unitary operators), the expansion is not truncated at all.

3.2.1 Update

The weight Eq. (3.9) of a specific state p and a sequence S_n can be extracted from the partition function Eq. (3.8). For the updates the weight has to be positive definite, otherwise the absolute value $|W(\alpha, S_n)|$ is used.

$$W(\alpha, S_n) = \frac{\beta^n (\tilde{L} - n)!}{\tilde{L}!} \langle \alpha | \prod_{i=1}^{\tilde{L}} \hat{h}_{a_i,b_i} | \alpha \rangle \tag{3.9}$$

We start the simulation with a sequence of unitary operators as initial state:

$$\{(0,0)_1, (0,0)_2, ..., (0,0)_{\tilde{L}}\}$$

For the diagonal updates, unitary operators are replaced by diagonal operators and vice versa with a certain probability using Metropolis-Hastings, Eqs. (3.10) and (3.11), assuring detailed balance [22], which causes a change of the number of diagonal operators n in the fixed sequence length $\tilde{L}$.

$$P[(0,0)_p \to (1,b)_p] = \frac{N\beta \langle \alpha_b(p) | \hat{h}_{1,b} | \alpha_b(p) \rangle}{\tilde{L} - n} \tag{3.10}$$

$$P[(1,b)_p \to (0,0)_p] = \frac{\tilde{L} - n + 1}{M\beta \langle \alpha_b(p) | \hat{h}_{1,b} | \alpha_b(p) \rangle} \tag{3.11}$$

The off-diagonal update is realized by directed loop updates, see Sandvik and Syljuåsen [22], which are a modification of worm updates (see Prokof'ev et al. [23]). The world line configuration is enlarged by an open line fragment, inserting an (S^-, S^+) operator pair at randomly chosen imaginary time (τ_{S^+}, τ_{S^-}). Moving one end or both ends (operator source, operator drain) randomly in space-time and accepting/ rejecting this by Metropolis-Hastings, gives local updates until the two ends of the worm meet again, annihilate and close the loop.

Possible maneuvers of the update are shown in Fig. 3.2.

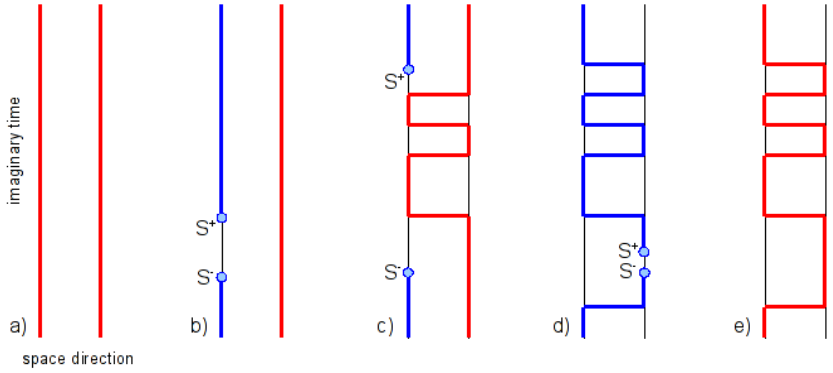

Figure 3.1: Example of a worm update: a) shows closed world lines, in b) an open line fragment (worm) is inserted with S^+ and S^- operator, jumping of the worm head is shown in c), in d) the two ends of the worm annihilate and e) gives the new world line configuration (red colored line means spin up)

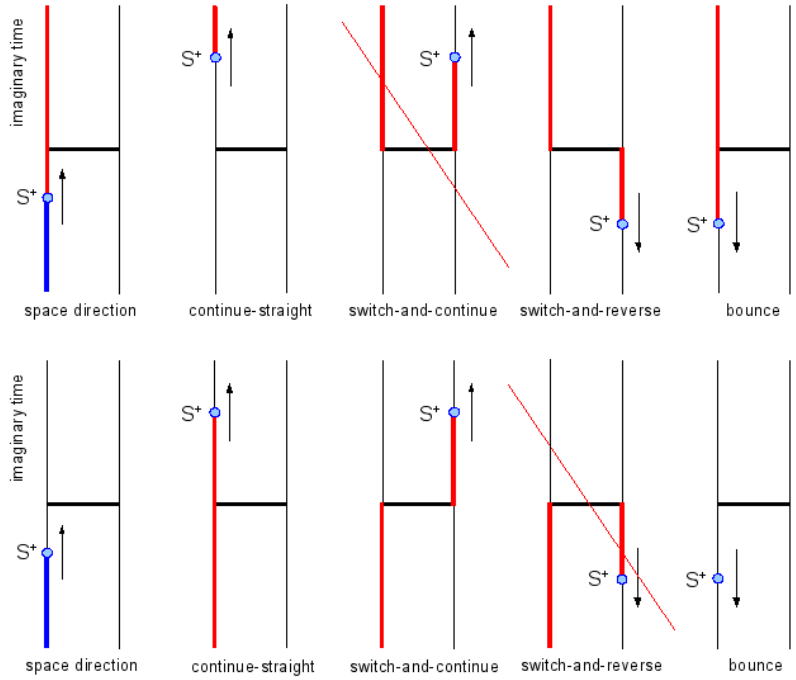

Figure 3.2: Examples of local updates: *continue-straight*, *switch-and-continue*, *switch-and-reverse* and *bounce* of a sample configuration. In the first case the *switch-and-continue* and in the second the *switch-and-reverse* maneuver is marked as forbidden.

3.3 SSE with static phonons

In this section we just have to describe a small adjustment between the SSE of the Heisenberg model (see Sec. 3.2) and the SSE of the Heisenberg model with static phonon interaction. The change of the Hamiltonian concerns the static spin-phonon coupling, a periodically alternating coupling. The adjustment is described by a function of the bond index b_i and the phonon displacement δ, as already mentioned above:

$$f(b_i) = \{1 + (-1)^{b_i}\delta\}$$

This causes a change in the matrix element in Eq. (3.8).

$$W(\alpha, S_n) = \frac{\beta^n(\tilde{L}-n)!}{\tilde{L}!} \langle\alpha| \prod_{i=1}^{\tilde{L}} f(b_i)\hat{h}_{a_i,b_i} |\alpha\rangle \tag{3.12}$$

Thus probabilities P of the Metropolis-Hastings- based update between unitary and diagonal operators change consequently.

$$P[(0,0)_p \to (1,b)_p] = \frac{N\beta \langle\alpha_b(p)| f(b_i)\hat{h}_{1,b} |\alpha_b(p)\rangle}{\tilde{L}-n} \tag{3.13}$$

$$P[(1,b)_p \to (0,0)_p] = \frac{\tilde{L}-n+1}{M\beta \langle\alpha_b(p)| f(b_i)\hat{h}_{1,b} |\alpha_b(p)\rangle} \tag{3.14}$$

On the other hand, the off-diagonal update, based on the worm update is not changed at all.

3.4 Mapping: SSE and continuous time

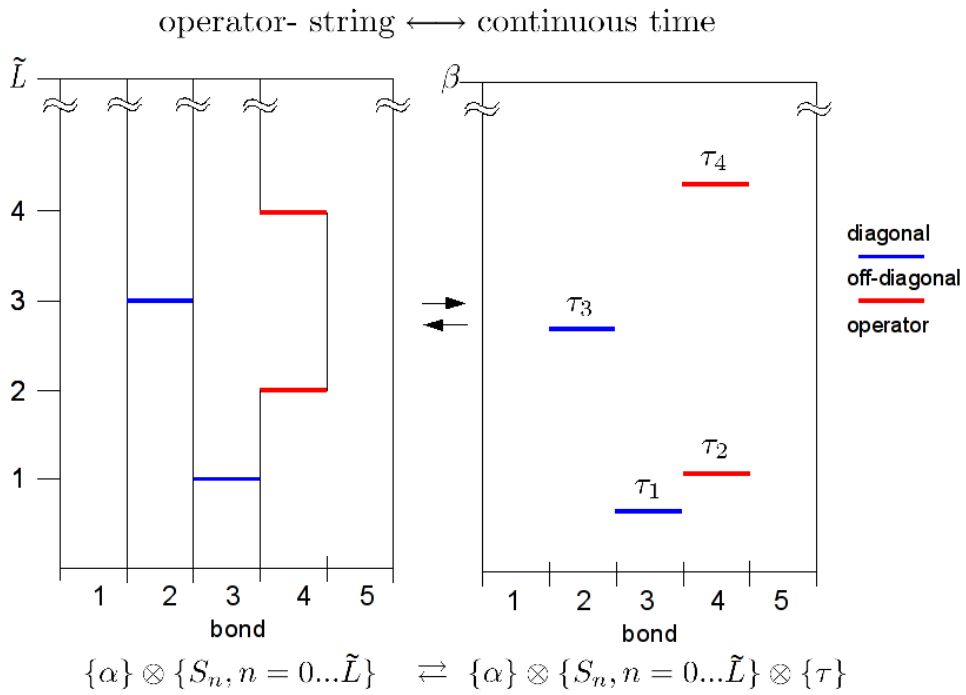

Figure 3.3: Mapping between SSE operator string index and continuous time

Starting by enlarging our configuration space

$$\{\alpha\} \otimes \{S_n, n = 0, ..., \infty\} \rightarrow \{\alpha\} \otimes \{S_n, n = 0, ..., \infty\} \otimes \{\tau\}$$

we treat our partition function by Trotter decomposition, introducing imaginary time τ.

$$\begin{aligned} Z &= \mathrm{Tr}\ e^{-\beta \hat{H}} \\ &= \mathrm{Tr}\ e^{\beta \sum_i \hat{h}_{a_i,b_i}} \\ &= \mathrm{Tr}\ \lim_{\Delta\tau \to 0} \left[e^{\sum_i \Delta\tau \hat{h}_{a_i,b_i}} \right]^{\frac{\beta}{\Delta\tau}} \\ &= \mathrm{Tr}\ \lim_{\Delta\tau \to 0} \left[\prod_i \left(1 + \Delta\tau \sum_i \hat{h}_{a_i,b_i} \right) \right]^{\frac{\beta}{\Delta\tau}} \end{aligned} \tag{3.15}$$

Analogous to Eq. (3.7) we rewrite the product of the sum of local operators by time ordering $\{\tau\} \rightarrow \tau_1 < \tau_2 < ... < \tau_{n-1} < \tau_n$ (operator acting at time τ_i) as a sequence of n non-unitary local operators.

$$Z = \sum_{\{\alpha\}} \lim_{\Delta\tau \to 0} \sum_{n=0}^{\frac{\beta}{\Delta\tau}} \sum_{\{S_n\}} \sum_{\{\tau\}} \Delta\tau^n \langle\alpha| \prod_i \hat{h}^{\tau}_{a_i,b_i} |\alpha\rangle \tag{3.16}$$

This gives the same shape of the partition function as Eq. (3.8). The sum of all time vectors can now be split up[6]:

$$\sum_{\{\tau\}} \Delta\tau^n = \sum_{\tau_n=0}^{\tau_n<\beta} \Delta\tau \sum_{\tau_{n-1}=0}^{\tau_{n-1}<\tau_n} \Delta\tau ... \sum_{\tau_1=0}^{\tau_1<\tau_2} \Delta\tau \tag{3.17}$$

Doing the limit $\Delta\tau \rightarrow 0$ leads to the time integrals in the partition function, which gives us the interaction representation:

$$Z = \sum_{\{\alpha\}} \sum_{n=0}^{\infty} \sum_{\{S_n\}} \int_0^{\beta} d\tau_n ... \int_0^{\tau_3} d\tau_2 \int_0^{\tau_2} d\tau_1 \langle\alpha| \prod_i \hat{h}^{\tau}_{a_i,b_i} |\alpha\rangle \tag{3.18}$$

When the local Hamiltonians of the sequence are time independent, evaluating the integrals gives a constant $\frac{\beta^n}{n!}$:

$$Z = \sum_{\{\alpha\}} \sum_{n=0}^{\infty} \sum_{\{S_n\}} \frac{\beta^n}{n!} \langle\alpha| \prod_i \hat{h}_{a_i,b_i} |\alpha\rangle \tag{3.19}$$

This is the same as Eq. (3.8) until

$$W(\alpha, S_n) = W(\alpha, S_n) \int_0^{\beta} d\tau_n ... \int_0^{\tau_3} d\tau_2 \int_0^{\tau_2} d\tau_1 \; p(\tau|n, \beta) \tag{3.20}$$

with the probability density $p(\tau|n, \beta)$ of the time vector τ.

$$p(\tau|n, \beta) := \frac{n!}{\beta^n} \tag{3.21}$$

[6] see Dyson time ordering operator, Nolting [24]

We can now do a stochastic mapping from an SSE to an imaginary time configuration. For every configuration (α, S_n) a sampling $\{\tau\}$ has to be chosen. This can be done in two different ways:

1) Draw n independent random points out of a uniform probability density ($p = 1/\beta^n$) in the interval $[0, \beta)$ and sort them from lower to higher time. There are $n!$ possible arrangements ($p = n!/\beta^n$), which gives us τ_i Poisson-points,
or as used in this thesis:
2) Choose $(n+1)$ intervals $\Delta\tilde{\tau}_i$ out of an exponential probability density:

$$p(\Delta\tilde{\tau}_i) = \exp(-\Delta\tilde{\tau}_i) \tag{3.22}$$

By normalizing the intervals from $[0, \beta)$ with

$$\Delta\tau_i = \frac{\beta}{\sum_{j=1}^{n+1} \Delta\tilde{\tau}_j \Delta\tilde{\tau}_i} \tag{3.23}$$

and calculating time steps

$$\tau_i = \sum_{j=1}^{i} \Delta\tau_j \tag{3.24}$$

we get τ_i Poisson points in a comfortable way too.

3.5 SSE with dynamic phonons

We start the derivation[7] with the Hamiltonian already described in Sec. 2.3.

$$H = \sum_{i=1}^{N} f(x_i)\mathbf{S}_i\mathbf{S}_{i+1} + H_p,$$
$$H_p = \sum_{q}^{1B.Z.} \frac{p_q^2}{2} + \frac{\omega^2(q)}{2}x_q^2 \tag{3.25}$$

The trace Tr_s of the partition function Eq. (3.2) is now written in spin space Eq. (3.26), in the basis of the diagonal part of the Hamiltonian. $\mathcal{D}x$ is the measure of the path integral over all phonon configuration $\{x_i(\tau)\}$ transformed from quantum mechanical displacement and momentum operator to classical variables ($x_i \to x_i(\tau)$, $p_i \to \frac{idx_i(\tau)}{d\tau}$) in imaginary time.

$$Z = \mathrm{Tr}_s \int \mathcal{D}x \, \exp\left(-\int_0^\beta d\tau H[\{x_i(\tau)\}]\right) \tag{3.26}$$

In this thesis we center our efforts on site phonons, but also bond phonons can be implemented in a similar way. In the following simulations we consider optical phonons, therefore dispersion-less Einstein phonons ω_0 are inserted.

$$f(x_i) = 1 + g \cdot (x_i - x_{i-1}) \tag{3.27}$$

Based on site and optical phonons, the transformed Hamiltonian is now written as:

$$H[\{x_i(\tau)\}] = \sum_{i=1}^{N}(1 + g \cdot (x_i(\tau) - x_{i+1}(\tau)))\left(S_iS_{i+1} + \frac{1}{4}\right) + H_p[\{x_i(\tau)\}]$$
$$H_p[\{x_i(\tau)\}] = \sum_{q}^{1B.Z.} \frac{1}{2}\left(-\dot{x}_q^2(\tau) + \omega_0^2 x_q^2(\tau)\right) \tag{3.28}$$

In a next step the partition function is written in the interaction representation, with H_{ph} staying in the exponent, following Sandvik et al. [19] and Prokof'ev [25] [8].

[7] based on the thesis of Michel [2]

[8] The statistical operator is related to a Matsubara [24] evolution σ: $\exp(-\beta\hat{H}) = \exp(-\beta H_0)\sigma$, where H_0 is the diagonal part of the Hamiltonian and expanded in the off-diagonal part

$$Z = \sum_{n=0}^{\infty} \sum_{S_n,\alpha} \int_{\tau_n} d\tau \times \int \mathcal{D}x \, \langle\alpha| \prod_{l=0}^{n} f(x_{s_l}(\tau_l)) \; \hat{h}^{\tau}_{a_l,s_l} \, |\alpha\rangle \times \exp\left(- \int_0^{\beta} d\tau H_p[x_i(\tau)] \right) \tag{3.29}$$

The spin-phonon coupling $f(x_{s_l})$ at site index s_l is then raised into the exponential function. This yields an effective action $S[\{x_i(\tau)\}, S_n^{\tau}]$ for a phonon configuration $\{x_i(\tau)\}$ and a specific operator sequence S_n^{τ}, Eq. (3.31).

$$Z = \sum_{n=0}^{\infty} \sum_{S_n,\alpha} \int_{\tau_n} d\tau \, \langle\alpha| \prod_{l=0}^{n} \hat{h}^{\tau}_{a_l,s_l} \, |\alpha\rangle \times \int \mathcal{D}x \, \exp\left(-S[x_i(\tau), S_n^{\tau}]\right) \tag{3.30}$$

$$S[\{x_i(\tau)\}, S_n^{\tau}] = \int_0^{\beta} d\tau H_p[\{x_i(\tau)\}] - \sum_{l=1}^{n} \ln(f(x_{s_l}(\tau_l))) \tag{3.31}$$

The logarithm part of the phonon effective action depends on the site s_l and imaginary time τ_l of the spin operators, as sketched in Fig. 3.4.

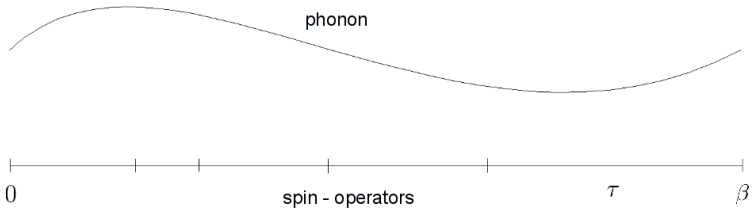

Figure 3.4: Phonon displacement at fixed spin operators

In order to get an efficient Monte-Carlo procedure, the logarithm is now expanded to first order, resulting in a bilinear action, from which a sample of a global new phonon configuration can be drawn exactly. We then accept or reject the proposal configuration to ensure detail balance with reference to the correct action Eq. (3.30).

$$\ln(f(x_{s_l})) = \ln(1 + g \cdot (x_{s_l}(\tau_l) - x_{s_{l+1}}(\tau_l))) = g \cdot (x_{s_l}(\tau_l) - x_{s_{l+1}}(\tau_l)) + \mathcal{O}((x_{s_l}(\tau_l) - x_{s_{l+1}}(\tau_l))^2) \tag{3.32}$$

$$S_{prop}[\{x_i(\tau)\}, S_n^\tau] = \int_0^\beta d\tau H_p[\{x_i(\tau)\}] - \sum_{l=1}^{n} g \cdot (x_{s_l}(\tau_l) - x_{s_{l+1}}(\tau_l)) \quad (3.33)$$

After Fourier transform of the phonon displacement in imaginary time and space Eq. (3.34), the proposal action S_{prop} contains the coefficient of $A_{q,n}$ in a quadratic way, Eq. (3.38).

$$x_l(\tau) = \frac{1}{\sqrt{L\beta}} \sum_{q}^{1B.Z.} \sum_{n=-\infty}^{\infty} A_{q,n} \exp(-i(lq + \tau\omega_n)) \quad (3.34)$$

By inserting a function $D(i,\tau)$, the spin dependent part of the proposal action will be forced to the time τ_l and space s_l of the spins.

$$D(i,\tau) := \sum_{l=1}^{n} \delta(\tau - \tau_l)\delta_{i,s_l} \quad (3.35)$$

$$S_{prop}[\{x_i(\tau)\}, S_n^\tau] = \int_0^\beta d\tau H_p[\{x_i(\tau)] - g \sum_{l=1}^{n} (x_{s_l}(\tau_l) - x_{s_l+1}(\tau_l))\ D(i,\tau) \quad (3.36)$$

This action can now be diagonalized in Fourier space. Inserting the Fourier transformed coefficients in Eq. (3.36)

$$\begin{aligned} A_{q,n} &= a_{q,n} + ib_{q,n} \\ A_{-q,-n} &= a_{q,n} - ib_{q,n} \\ D_{q,n} &= \zeta_{q,n} + i\gamma_{q,n} \end{aligned} \quad (3.37)$$

the proposal action S_{prop} results in a quadratic form:

$$\begin{aligned} S_{prop}[\{a_{q,n}, b_{q,n}\}, S_n^\tau] = \sum_{q}^{1B.Z.} \sum_{n=0}^{\infty} \left(\alpha_{q,n} a_{q,n} + \frac{\acute{\alpha}_{q,n}}{2\alpha_{q,n}}\right)^2 + \\ \left(\alpha_{q,n}\beta_{q,n} + \frac{\acute{\beta}_{q,n}}{2\alpha_{q,n}}\right)^2 - \left(\frac{\acute{\alpha}_{q,n}}{2\alpha_{q,n}}\right)^2 - \left(\frac{\acute{\beta}_{q,n}}{2\alpha_{q,n}}\right)^2 \end{aligned} \quad (3.38)$$

$$\begin{aligned}
\alpha_{q,n}^2 &= \omega_n^2 + (1 - 0.5\ \delta_{n,0})\omega_0^2 \\
\acute{\alpha}_{q,n} &= -g(2 - \delta_{n,0})(\zeta_{k,n}(1 - \cos(k)) - \gamma_{k,n}\sin(k)) \\
\acute{\beta}_{q,n} &= -g(2 - \delta_{n,0})(\zeta_{k,n}\sin(k) + \gamma_{k,n}(1 - \cos(k)))
\end{aligned} \tag{3.39}$$

Using Eq. (3.39) the physical action Eq. (3.31) becomes:

$$S[\{a_{q,n}, b_{q,n}\}, S_n^\tau] = \sum_{q}^{1B.Z.} \sum_{n=0}^{\infty} \alpha_{q,n}^2 (a_{q,n}^2 + b_{q,n}^2) - \sum_{l=1}^{n} \ln(1 + g \cdot (x_{s_l}(\tau_l) - x_{s_l+1}(\tau_l))) \tag{3.40}$$

The infinite limits of the sums (Matsubara frequencies) are truncated ($\infty \to n_m$) for simulation.

3.5.1 Phonon update

For the phonon update we use a fixed spin configuration and therefore pay attention to the partition function Eq. (3.30), where all phonon dependent parts are raised up to an exponential function. By observing the fraction of the weights of the new and old configuration for the updates, the unchanged spin parts do not contribute. The new proposed phonon configuration is drawn out of the distribution:

$$P(\{\acute{a}_{q,n}, \acute{b}_{q,n}\}) = \exp(-S_{prop}[\{\acute{a}_{q,n}, \acute{b}_{q,n}\}, S_L^\tau]) \tag{3.41}$$

After bilinearization of the effective action's coefficients, where x_d is normally distributed generated, the proposal amplitude is Gaussian distributed, see Fig. 3.5.

$$\begin{aligned} \acute{a}_{q,n} &= \frac{x_d}{\alpha_{q,n}} - \frac{\acute{\alpha}_{q,n}}{2\alpha_{q,n}^2} \\ \acute{b}_{q,n} &= \frac{x_d}{\alpha_{q,n}} - \frac{\acute{\beta}_{q,n}}{2\alpha_{q,n}^2} \end{aligned} \tag{3.42}$$

The new amplitudes are accepted or rejected by evaluating the Metropolis-Hastings probability, concerning the effective- and the proposal effective actions:

$$\begin{aligned} P(a_{q,n}, b_{q,n} \to a'_{q,n}, b'_{q,n}) = \exp(&-S[a'_{q,n}, b'_{q,n}] + S[a_{q,n}, b_{q,n}] \\ &- S_{prop}[a_{q,n}, b_{q,n}] + S_{prop}[a'_{q,n}, b'_{q,n}]) \end{aligned} \tag{3.43}$$

Switching between the space of Matsubara frequencies and imaginary time needs a Fourier transform. This leads to a time discretization t_i. To project the time slice t_i to the operator string based time τ_l, a linear approximation between the highest time slice $t_l^\downarrow$ (lower than τ_l) and the lowest time slice $t_l^\uparrow$ (higher than τ_l) is done:

$$x'_{s_l}(\tau_l) = x'_{s_l}(t_l^\downarrow) + \frac{x'_{s_l}(t_l^\uparrow) - x'_{s_l}(t_l^\downarrow)}{t_l^\uparrow - t_l^\downarrow}(t_l - t_l^\downarrow) \tag{3.44}$$

The momentum/Matsubara-frequency-space is split up into subdivisions of simultaneously updated amplitudes, with decreasing partitions around the critical and observable most interesting area ($q = \pi, \omega_n = 0$) to improve the acceptance probability.

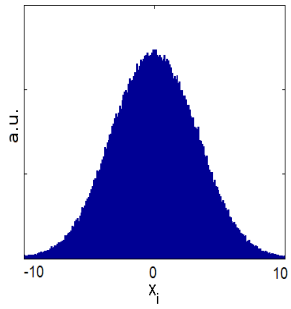

Figure 3.5: Gaussian distribution of the phonon state x_i (snapshot of one site during a simulation)

3.5.2 Spin update

For the spin update the phonon configuration is fixed. Let's have a look at the necessary modifications of Sec. 3.2. Concerning the spin-phonon interaction $f(x_{s_l}(\tau_l))$, the weight of the spin configuration $W_s(\alpha, S_n^\tau \mid x_i(\tau))$ can be extracted from an equation similar to Eq. (3.29).

$$W_s(\alpha, S_n^\tau \mid x_i(\tau)) = \frac{(\tilde{L}-n)!n!}{\tilde{L}!} \langle\alpha| \prod_{l=0}^{n} f(x_{s_l}(\tau_l))\ \hat{h}^\tau_{a_l,s_l} |\alpha\rangle \tag{3.45}$$

The off-diagonal update does not depend on the phonon configuration and is realized with the already described worm algorithm $\hat{h}^\tau_{a_l,s_l} : \hat{h}_{1,sl} \leftrightarrow \hat{h}_{2,sl}$. The diagonal one ($\hat{\mathbb{1}} \leftrightarrow \hat{h}_{1,s_l}$) is done by acceptance depending on the Metropolis-Hastings probabilities:

$$\begin{aligned} P(\hat{h}^\tau_{a_l,s_l} : \hat{\mathbb{1}} \to \hat{h}_{1,s_l}) &= \frac{W_s(\hat{h}^\tau_{a_l,s_l} = \hat{h}_{1,s_l})}{W_s(\hat{h}^\tau_{a_l,s_l} = \hat{\mathbb{1}})} \frac{1}{P(s_l)P(\tau_l)} \\ P(\hat{h}^\tau_{a_l,s_l} : \hat{h}_{1,s_l} \to \hat{\mathbb{1}}) &= \frac{W_s(\hat{h}^\tau_{a_l,s_l} = \hat{\mathbb{1}})}{W_s(\hat{h}^\tau_{a_l,s_l} = \hat{h}_{1,s_l})} P(s_l)P(\tau_l) \end{aligned} \tag{3.46}$$

were probabilities higher than one are set to one. The underlying bond s_l is drawn out of a uniform probability density $P(s_l) = \frac{1}{N}$ and the probability density for the time τ_l is constructed out of the difference between the next highest $\tau_l^\uparrow$ and next lowest time $\tau_l^\downarrow$ of a non unitary operator (def. $\tau_1^\uparrow = \beta$ and $\tau_n^\downarrow = 0$).

This gives us the following Metropolis-Hastings probabilities:

$$P(\hat{h}^{\tau}_{a_l,s_l} : \hat{\mathbb{1}} \to \hat{h}_{1,s_l}) = \langle\alpha(l)|\, f(x_{s_l}(\tau_l))\ \hat{h}_{1,s_l}\, |\alpha(l-1)\rangle\, \frac{N(n+1)(\tau_l^{\uparrow} - \tau_l^{\downarrow})}{\tilde{L} - n} \tag{3.47}$$

$$P(\hat{h}^{\tau}_{a_l,s_l} : \hat{h}_{1,s_l} \to \hat{\mathbb{1}}) = \langle\alpha(l)|\, f(x_{s_l}(\tau_l))\ \hat{h}_{1,s_l}\, |\alpha(l-1)\rangle^{-1}\, \frac{\tilde{L} - n + 1}{Nn(\tau_l^{\uparrow} - \tau_l^{\downarrow})} \tag{3.48}$$

The time of the spin-phonon interaction part is again linearly approximated by the operator string time τ_l.

3.6 Tempering

For large phonon couplings, especially in the two-dimensional case, the simulation may get stuck in a local minimum[9].

To handle this local minimum problem we implement tempering in our calculations:

The purpose of this tempering procedure, with respect to the spin-phonon coupling constant g, is to link configurations suffering from high autocorrelation (simulations with high g) to simulations with lower autocorrelation (with lower g). The range of the coupling is defined by a maximum coupling, that respresents the highest parameter of interest for the simulation we intend to determine and a minimum coupling at which the system rapidly equilibrates. The shifted configurations are accepted or rejected by a Metropolis Hastings decision. The best way to choose the steps of the coupling would be to improve the Metropolis Hastings acceptance for the exchange. To avoid 'useless' extrawork every simulation (every coupling step) will do measurements with this exchanged configurations.

In detail tempering is realized in the following way:

A number of parallel processes (nop), seen as a closed process chain with slightly different phonon coupling constants $g_0 < ... \; g_{nop} < g_{nop_{max}}$ is started. g_0 is chosen low enough, so that the configurations do not suffer from high autocorrelation anymore. After a few hundred[10] sweeps the configurations and site states are shifted to a neighbor process, either to the left ($nop \rightarrow nop-1$) or to the right ($nop \rightarrow nop+1$) neighbor, Fig. 3.6. I.e. configurations suffering from high autocorrelations are shifted to calculations with lower phonon coupling constants and vice versa. The new configuration suggestion is accepted or rejected by Metropolis Hastings in one of the two involved processes. A flag will show the second process to accept or reject the new configuration too. Thereby configurations are shifted in the process chain and serve as proposal configurations, but no one will be discarded.

[9]Indication of a local minimum problem: Although no site is specially preferred, the mean value of the phonon coordinate is far away from zero. Moreover large autocorrelations for all observables appear.

[10]These chosen number of sweeps depends on the system size; for a 4x4 Spin-system we used 100 sweeps (empirically determined).

The Metropolis Hastings decision of a process is done with the following probability (γ old configuration and ξ new configuration):

$$
\begin{aligned}
p(g_\gamma \to g_\xi) &= \frac{W(\alpha_\xi, S^{\tau_\xi}_{n_\xi}(g_\xi))}{W(\alpha_\gamma, S^{\tau_\gamma}_{n_\gamma}(g_\gamma))}, \\
W(\alpha_\xi, S^{\tau_\xi}_{n_\xi}) &= \frac{(\tilde{L}_\xi - n_\xi)! n_\xi!}{\tilde{L}_\xi!} \langle \alpha_\xi | \prod_{l=0}^{n_\xi} f(x_{s_l\xi}(\tau_{l\xi})|g_\xi) \hat{h}^{\tau_\xi}_{a_l,s_l} |\alpha_\xi\rangle , \\
W(\alpha_\gamma, S^{\tau_\gamma}_{n_\gamma}) &= \frac{(\tilde{L}_\gamma - n_\gamma)! n_\gamma!}{\tilde{L}_\gamma!} \langle \alpha_\gamma | \prod_{l=0}^{n_\gamma} f(x_{s_l\gamma}(\tau_{l\gamma})|g_\gamma) \hat{h}^{\tau_\gamma}_{a_l,s_l} |\alpha_\gamma\rangle ,
\end{aligned} \tag{3.49}
$$

After that, the next hundred sweeps are done. With respect to the Metropolis Hastings decisions configurations and site states are shifted to other sites in the 'process chain'. After several thousand exchanges[11], the configurations and expectation values do not suffer from high autocorrelation anymore. Thus the local minimum problem is corrected.

Technical details:

Initially the exchange of the configuration, the site states and the elements of the operator string (Fig. 3.7) have been realized by *OpenMPI* a Message Parsing Interface. MPI [26] is a communication protocol, which makes it possible for processors to synchronize and exchange messages to each other in an efficient way. Due to fundermental conflicts with the used ALPS libraries used in the implementation and compiling phase (even with other MPI versions) we were forced to chose an less efficient way to go on.

Subsequently the synchronized configuration exchange was realized in the following way: The configurations, the site state and the elements of the operator string are written into a file. Renaming this file with a sweep-index based file name gives a sign to read the parameters, attributes and flags for the next process, which checks its existence. Deleting this file after the reading will set a flag to the former process, which checks its nonexistence. During the existence checks (synchronization) the processes have to wait. Finally, exchanging the operator string causes a dynamical adjustment of its length $\tilde{L}$.

[11] To get good statistic the choice of the total amount of sweeps has to be empirically determined by observing the observables and their autocorrelation time during the simulation.

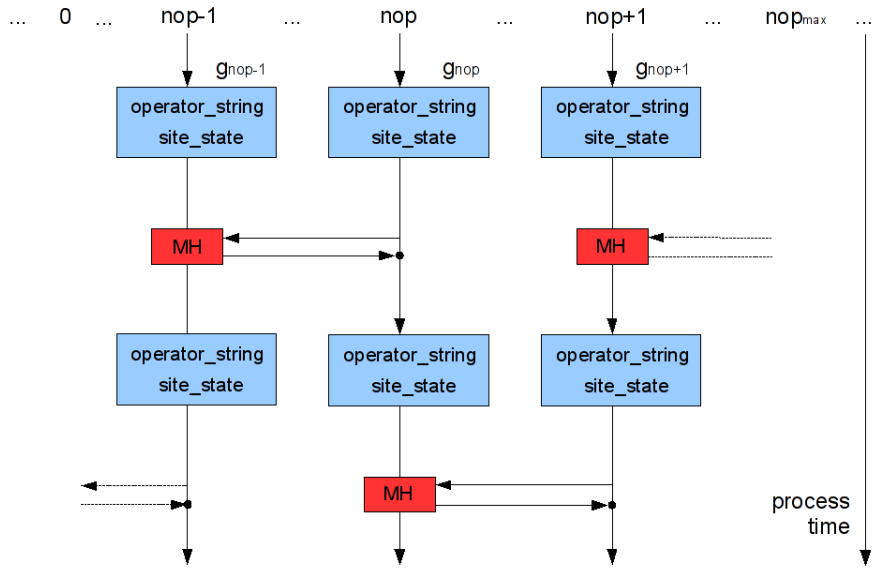

Figure 3.6: Process handling and communication during the tempering: In specific steps an exchange of the operator string and the site states between different processes (number of process, nop) characterized by specific phonon interactions g_{nop} happens. The acceptance of this exchange is done by Metropolis Hastings (MH)

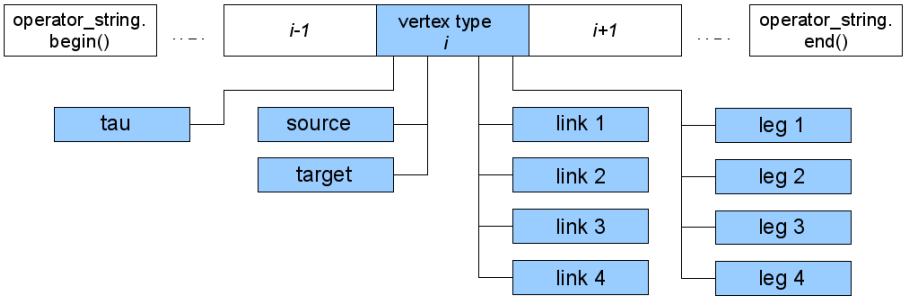

Figure 3.7: Elements of the operator string and some control flags have to be exchanged during the tempering between the processes

In the operator string the kind of the operator (unitary, diagonal and off-diagonal) and its information of the spin alignment are represented by a vertex of 4 legs, shown in case of a diagonal operator in Fig. 3.8. The 'link' data, Fig. 3.8, gives the positioning of this operator and τ the corresponding imaginary time it acts in.

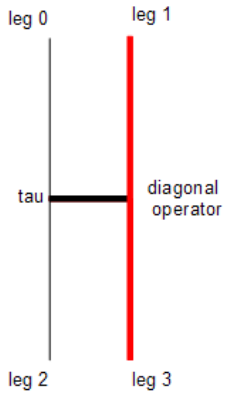

Figure 3.8: Linked vertex representation (red color means spin up)

Problems in parallelization:

The Network File System (used in our cluster) issues no guarantee of the chronology of the file access and no guarantee for the duration of treating atomic and non-atomic operations like the 'delete' command. This causes a problem, if the number of processes is necessarily larger than the maximum core number of the computer in the cluster (leaving the shared cache).

3.7 Expectation value

The diagonal expectation values can now be determined in the following way:

$$\langle \hat{A} \rangle = \frac{\sum_C A(C)W(C)}{\sum_C W(C)} \tag{3.50}$$

where $A(C)$ is the estimator and $W(C)$ the weight of the specific sampling configuration. The notation distinguishes whether the phonon subspace is used for dynamic phonon calculations.

$$\begin{aligned} W(C) &= W(\alpha, S_n) \\ W(C) &= W(\alpha, S_n^\tau, x_i(\tau)) \end{aligned} \tag{3.51}$$

For some configurations, like in geometrical frustrations of the lattice, the weight might not be positive definite. This causes the SIGN PROBLEM [21]. Avoiding negative weights, the sampling is done by using the absolute value of the weight and incorporating the sign into the observables. In many sign problem- appearing cases the usage of Monte-Carlo is unrewarding. The QMC will get exponentially slow, the average sign of the configurations will decrease exponentially to zeros and the statistical errors of observables will increase exponentially. In the simulations of this thesis no sign problem appears.

The statistical error of correlated observables is calculated by evaluating the variance of the observable including the autocorrelation time with the series length n, see Evertz [27].

$$\begin{aligned} \Delta\hat{A} &= \sqrt{\frac{\sigma^2_{\hat{A}}}{n}\, 2\tau_{int}(\hat{A})} \\ \sigma^2_{\hat{A}} &= \langle \hat{A}^2 \rangle - \langle \hat{A} \rangle^2 \end{aligned} \tag{3.52}$$

In order to determine the integrated autocorrelation time τ_{int} binning is used[12]. The time series of observables is cut into blocks with increasing lengths. Block-length by block-length the variance is calculated and converges to the exact variance when block averages are uncorrelated and the block length greatly exceeds the correlation time.

[12]Binning for error calculations as well as jackknife for cross-correlation analysis is already implemented in the ALPS libraries [20].

The expectation value of the energy of the pure Heisenberg model and for the static phonon interaction depends only on $\tilde{L}$ defined by SSE, see Sandvik et al. [19].

$$\langle E \rangle = -\frac{1}{\beta} \langle \tilde{L} \rangle_{W(C)} \tag{3.53}$$

For the dynamic phonon interaction case (see Michel [2]), with respect to the weight of the configuration and the truncation of the Matsubara frequencies n_m, the expectation value $\langle E \rangle$ is found by:

$$\langle E \rangle = \frac{1}{\beta} \left\langle \tilde{L} + \frac{L(2n_m - 1)}{\beta} - \sum_{q}^{1.B.Z.} \sum_{n=1}^{n_m} \frac{8n^2\pi^2}{\beta^2} (a_{q,n}^2 + b_{q,n}^2) \right\rangle_{W(C)} \tag{3.54}$$

3.8 Green's function

We have discussed the algorithm with the updates and how to calculate expectation values of observables. Now we want to get a closer look at the dynamics of the model by measuring the imaginary time dependent correlation functions - Green's functions. Starting with their definition:

$$G_{BA}(\tau) := \langle \hat{B}_\tau \hat{A}_0 \rangle := \langle e^{\tau \hat{H}} \hat{B} e^{-\tau \hat{H}} \hat{A} \rangle = \frac{1}{Z} \mathrm{Tr} \left\{ e^{-(\beta - \tau)\hat{H}} \hat{B} e^{-\tau \hat{H}} \hat{A} \right\} \tag{3.55}$$

In this thesis the operators $\hat{A}$ and $\hat{B}$ will be e.g. S_i^z and S_j^z, which means the operators are diagonal in the basis $\{|\alpha\rangle\}$. The correlation of the operators are evaluated for different times, where $\langle B_{t'} A_t \rangle = \langle B_0 A_{t-t'} \rangle$ can be rearranged, see Nolting [24]. Treating the Green's function with the Trotter decomposition as done in Sec. 3.4, the correlation function is measured by using the fast Fourier transform, using a discrete time grid with spacing of $\delta\tau$. For diagonal operators the correlation function can be rewritten in terms of (see Michel [2]):

$$G_{BA}(\tau) = \frac{1}{Z} \sum_{\{\alpha\}} \lim_{\Delta\tau \to 0} \sum_{n=0}^{\beta/\Delta\tau} \Delta\tau^n \sum_{S_n^\tau} \langle \alpha | \prod_{i}^{\tau_i \geq \tau} \hat{h}_{a_i,b_i}^\tau \hat{B} \prod_{i}^{\tau_i \leq \tau} \hat{h}_{a_i,b_i}^\tau \hat{A} \, | \alpha \rangle \tag{3.56}$$

Next a time spacing index $l \in [0, \beta/\delta\tau - 1]$ is inserted.

$$G_{BA}(l\delta\tau) = \frac{1}{Z}\sum_{\{\alpha\}}\lim_{\Delta\tau\to 0}\sum_{n=0}^{\beta/\Delta\tau}\Delta\tau^n\sum_{S_n^\tau}\langle\alpha|\prod_i^n \hat{h}^\tau_{a_i,b_i}|\alpha\rangle\langle\alpha_{l\delta\tau}|\hat{B}|\alpha_{l\delta\tau}\rangle\langle\alpha_0|\hat{A}|\alpha_0\rangle \tag{3.57}$$

Evaluating the limit $\Delta\tau \to 0$ like in Sec. 3.4 will give us the integral formulation of the time dependent part.

$$\begin{aligned}
&G_{BA}(l\delta\tau) = \\
&= \frac{1}{Z}\sum_{\{\alpha\}}\sum_{n=0}^{\infty}\sum_{S_n^\tau}\langle\alpha|\prod_i^n \hat{h}^\tau_{a_i,b_i}|\alpha\rangle\int_0^\beta d\tau_n \ ... \int_0^{\tau_2} d\tau_1 \langle\alpha_{l\delta\tau}|\hat{B}|\alpha_{l\delta\tau}\rangle\langle\alpha_0|\hat{A}|\alpha_0\rangle \\
&= \frac{1}{Z}\sum_{\{\alpha\}}\sum_{n=0}^{\infty}\sum_{S_n^\tau} W(\alpha,S_n)\int_0^\beta d\tau_n \ ... \int_0^{\tau_2} d\tau_1 \ p(\tau|n,\beta)\langle\alpha_{l\delta\tau}|\hat{B}|\alpha_{l\delta\tau}\rangle\langle\alpha_0|\hat{A}|\alpha_0\rangle
\end{aligned} \tag{3.58}$$

In a short way the Green's function can be written as:

$$G_{BA}(l\delta\tau) = \langle B((j,l\delta\tau),\alpha,S_n,\tau)A((i,0),\alpha,S_n,\tau)\rangle_{W(\alpha,S_n),p(\tau|n,\beta)} \tag{3.59}$$

where operator $\hat{B}$ is acting at time $l\delta\tau$ and bond j and operator $\hat{A}$ acting at time 0 and bond j. Due to translation invariance in time and space the fast Fourier transform can be used.

$$\tilde{f}(k,\omega) = \sqrt{\frac{\delta\tau}{\beta L}}\sum_{\nu}^{\beta/\delta\tau}\sum_{j}^{N} f(\nu,j)e^{-i\nu\omega\frac{2\pi\delta\tau}{\beta}}e^{-i2\pi jk} \tag{3.60}$$

The correlation function is obtained as a convolution.

$$\tilde{G}_{BA}(\omega,k) = \sqrt{\frac{\delta\tau}{\beta}}\langle\tilde{B}((\omega,k),\alpha,S_n,\tau)\tilde{A}((\omega,k),\alpha,S_n,\tau)\rangle_{W(\alpha,S_n)p(\tau|n,\beta)} \tag{3.61}$$

In the following chapters the Fourier transformed spin operator $S^z_{k,\omega}$, already in ALPS implemented, is used for the spin correlation function $\langle S^z_{i,0}S^z_{j,\tau}\rangle$ calculations.

3.8.1 Phonon Green's function

The phonon spectra can be measured in a direct way, because the update is already realized in reciprocal space. The Green's function, a convolution after fast Fourier transform in space and imaginary time, can be calculated in the following way:

$$\begin{aligned} G_x(q,\omega_n) &= FT(\langle x_l(0)x_m(\tau)\rangle) \\ &= \left\langle \frac{1}{L\beta} \sum_{q,\acute{q}}^{1.B.Z.} \sum_{n,\acute{n}=-\infty}^{\infty} A_{q,n} e^{-i(lq)} A_{\acute{q},\acute{n}} e^{-i(m\acute{q}+\tau\omega_{\acute{n}})} \right\rangle \\ &= \langle A_{q,n} A_{-q,-n}\rangle = \langle a_{q,n}^2 + b_{q,n}^2\rangle \end{aligned} \tag{3.62}$$

For a jackknife[13] error analysis the series of observables is cut into blocks with similar lengths. The variance in relation to the average of the series is evaluated each time by leaving out one block. The variance of the cross-correlated observable is proportional to the mean of the evaluated variance series, see Evertz [27].

3.8.2 Maximum Entropy

The Maximum Entropy analysis is used to evaluate the inverse Laplace transform of the given imaginary time Green's function $G(\tau)$.

$$\underbrace{G(\tau)}_{\text{correlated, data with errors}} = \int_0^\infty A(\omega) \underbrace{K(\omega)}_{\text{kernel}}\, d\tau \tag{3.63}$$

The MaxEnt reconstructs the real frequency spectral function $A(\omega)$, using theory of probability (see von der Linden [28], Silver et al. [29])[14].
The analysis is based on the Bayes theorem,

$$p(A(\omega)|G(\tau),C,H) = \frac{p(G(\tau)|A(\omega),C,H)\ p(A(\omega)|C,H)}{p(G(\tau)|C,H)} \tag{3.64}$$

where the likelihood function $p(G(\tau)|A(\omega),C,H)$ describes the error statistics of the QMC, the prior probability $p(A(\omega)|C,H)$ contains the prior knowledge and the posterior probability reads like $p(A(\omega)|G(\tau),C,H)$. H stands

[13] included in ALPS

[14] Because of the ill-conditioned equation Eq. (3.63), the solution of $A(\omega)$ treated with direct inversion will be negligible to the prevalent noise.

for the hypothesis, containing the prior knowledge and C the underlying correlated errors in form of the error covariance matrix. For the prior a Poisson distribution is suggested, where adding small parts ΔA to $A(\omega)$ provides independence to already added values. Treating this probability with Stirling's formula leads to the Shannon-Entropy. Assuming the maximized entropy as a small peak the norm of the prior can be calculated via steepest decent approximation. Coupling an additive noise (a multivariate normal distribution) to the likelihood yields a convenient posterior[15].

The choice of the kernel $K_i(\omega)$ depends on the underlying spectral function $A(\omega)$ we expect to evaluate. For the spin spectral function we use following kernel:

$$K_{spin}(\omega) = \frac{e^{-\omega\tau} + e^{-\omega(\beta-\tau)}}{1 + e^{-\omega\beta}} \tanh\left(\frac{\beta\omega}{2}\right) \tag{3.65}$$

and for the phonon spectral functions obtaining $G(\omega)$ instead of $G(\tau)$:

$$K_{phonon}(\omega) = \frac{\omega}{\omega^2 + \tau^2} \tanh\left(\frac{\beta\omega}{2}\right) \tag{3.66}$$

[15]The evaluation is done by the MaxEnt program of W. von der Linden, D. Neuber and M. Hohenadler

Chapter 4

Heisenberg chain with static phonon interaction

Based on recent results of Sirker et al. [4] we start our investigation with the Heisenberg model with static phonon interactions, introduced in Sec. 2.2. A Spin-Peierls transition will occur if magnetic energy is gained by static distortion δ of the classical lattice. In the paper of Sirker et al. following Hamiltonian was used

$$H = J \sum_{j=1}^{N} \{1 + (-1)^j \delta\} \, \mathbf{S}_j \mathbf{S}_{j+1} + \frac{NK\delta^2}{2} \tag{4.1}$$

The first part describes the magnetic- E_{mag}, the second part the elastic E_{el} contribution. In the antiferromagnetic case a gain in magnetic Energy $E_{mag} \sim -\delta^{4/3}$, a cost in elastic energy $E_{el} \sim \delta^2$ and a gap of $E_g \sim \delta^{2/3}$ appears [30], treating the phonons in a mean-field random-phase approximation (RPA). That means, the antiferromagnet is unstable against static distortion, which is called the 'Peierls instability'.

Antiferromagnetic coupling:

$$\boxed{\begin{aligned} E_{mag} &\sim \delta^{4/3} \\ E_{el} &\sim \delta^2 \\ E_g &\sim \delta^{3/2} \end{aligned}} \tag{4.2}$$

In the ferromagnetic case calculations with modified spin wave theory (MSWT) lead to a gain in magnetic energy $E_{mag} \sim -T^{3/2}\delta^2$ and cost in elastic energy of similar form $E_{el} \sim E_{mag}$ [4]. It depends on the prefactor

and on the temperature T whether a finite δ is energetically favorable.

Ferromagnetic coupling:

$$\boxed{\begin{aligned} E_{mag} &\sim -T^{3/2}\delta^2 \\ E_{el} &\sim E_{mag} \\ E_g &\sim \text{ dep. on prefactor} \end{aligned}} \tag{4.3}$$

In contrast to the antiferromagnetic case there will be no transition in the ferromagnet in zero temperature limit, see Eqs. 4.3 and 4.2.

In Fig. 4.1 a phase diagram of the FM and AM chain is shown, evaluated by the use of density-matrix renormalization group applied to transfer matrices (TMRG) in Sirker [4]. To minimize the free energy and to determine a critical effective elastic constant $K_0(T)$ the phonon displacement $\delta(T)$ is treated as a thermodynamic degree of freedom. For a fixed phonon displacement δ the dimerization will occur if and only if $K < K_0(T)$ and $g > g_0(T)$[1]. The inset (b) in Fig. 4.1 shows the temperature dependence of the phonon displacement $\delta(T)$ of the FM chain. It jumps to $\delta(T) = 1$ when $K < K_0(T)$ for the temperature regime lower than the critical point TCP. At higher temperature T $\delta(T)$ shows a continuous behavior. Therefore a change between first and second order phase transition can be seen.

In order to verify this phase diagram for the FM chain calculations have been done by QMC for some temperatures and static phonon displacements[2]. To measure the dimerization an order parameter is used, which is a comparison between next-nearest neighbor energies:

$$\Delta_{SS}^{-} = \langle \mathbf{S}_{2i}\mathbf{S}_{2i+1} - \mathbf{S}_{2i}\mathbf{S}_{2i-1} \rangle \tag{4.4}$$

The coupling of the static phonons is related to the site index and therefore measuring $\mathbf{S}_i\mathbf{S}_{i+1}$ is not translational invariant[3]. In Fig. 4.2 the order parameter as a function of static phonon displacement δ and the temperature T is shown[4].

[1]The effective critical elastic constant relates to $K_0 = \tilde{K}J^2a_0^2/(4g_0^2)$ and $\tilde{K}$ to $E_{el} = N\tilde{K}u^2/2$, see Sec. 2.2.

[2]In the following simulations the truncated (SSE) expansion limit $\tilde{L}$ is chosen in the range of the system size times inverse temperature ($\tilde{L} \sim L\beta$). To obtain convergence and good statistics for the used observables and correlations we suggest, empirically evaluated, to use $L \cdot 10^5$ sweeps and to reject 10% for thermalization.

[3]The spin is measured in z direction, no direction in space is preferred. Therefore we get $\rightarrow \langle \mathbf{S_i S_j} \rangle = 3\langle S_i^z S_j^z \rangle$.

[4]The results in Fig. 4.2 agree with those obtained with TMRG by Sirker [4]

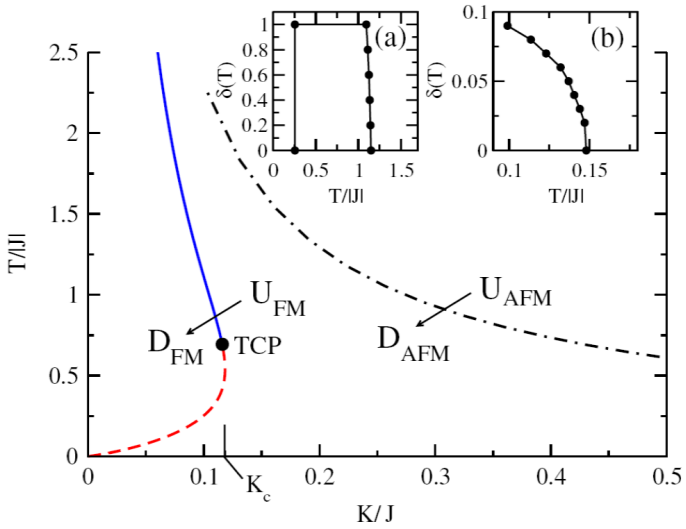

Figure 4.1: Phase diagram (by TMRG) of a dimerized AFM (black dashed curve) and a dimerized FM chain (blue/red curve). D_{FM} resp. D_{AFM} are the dimerized regimes, U_{FM} resp. U_{AFM} are the non-dimerized (uniform) ones. The FM chain has a second order (blue solid curve) and a first order phase transition (red dashed curve) separated by a critical point TCP. The insets show the behavior of the order parameter of the FM chain (a) at $K/|J| = 0.1$ and of the AFM chain (b) at $K/J = 2$. Taken from the paper of Sirker et. al. [4]

Increasing δ to 1 for higher temperature like $T = 1$, the order parameter Δ_{SS}^{-} rises almost in a linear way. On the other hand for lower temperatures like $T = 0.04$ the parameter keeps almost to zero until $\delta = 0.6$ and afterwards rises sharply to the triplet[5] energy of the spin-1/2 system. Quite interesting detail: because of higher excitation, the data points of $T = 1$ do not end exactly at the triplet energy of the system. Appendix A shows results of the order parameter for the spin-1-Heisenberg model.
In Fig. 4.3 the site energy of the Heisenberg chain is shown as a function of the displacement δ for a system at inverse temperature $\beta = 32$. This is almost in the lowest temperature regime of the phase diagram Fig. 4.1.

The site energy E for this low temperature stays more or less constant under variation of the displacement δ. Although there is no visible energy change for higher δ we are going to have a closer look at the $S^z S^z$ correlation by applying the 'Maximal Entropy Method' Sec. 3.8.2 to the evaluation of

[5] At $\delta = 1$ only two and two spins are coupled in the chain together.

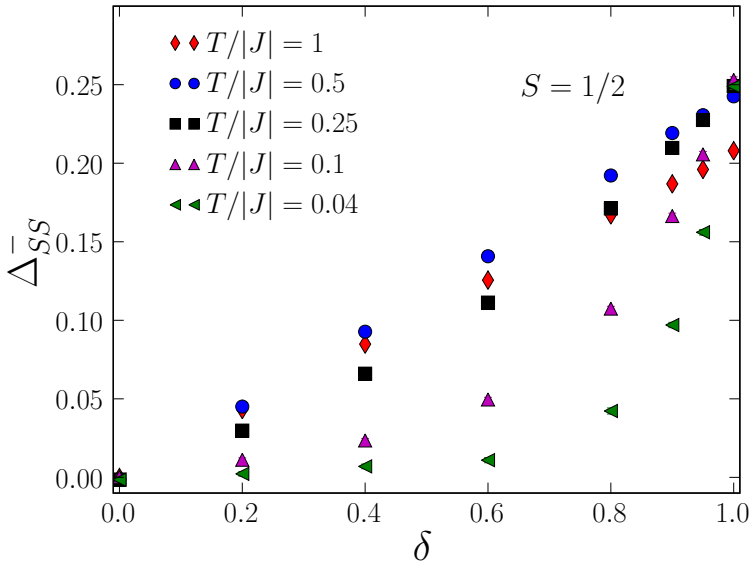

Figure 4.2: Spin order parameter Δ^{-}_{SS} for Spin 1/2, $J = -1, L = 128$, the errorbars are smaller than the symbols

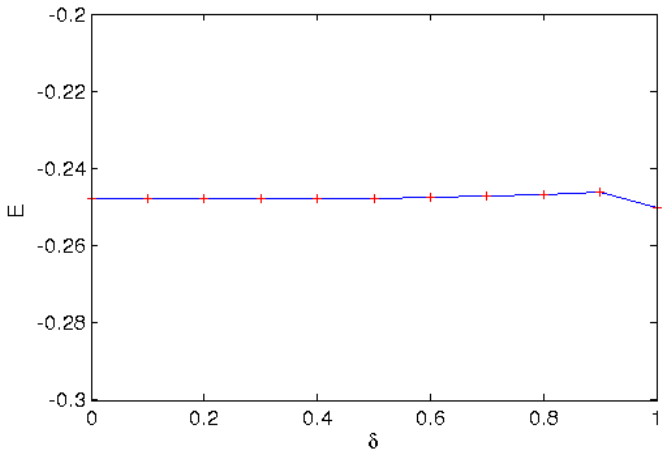

Figure 4.3: Site energy E of the Heisenberg chain vs. static phonon displacement $\delta, J = -1, \beta = 32, L = 128, \Delta E = 10^{-4}$

the Spectral function, see Fig. 4.4. For higher displacement δ the peaks of the spectral function broaden, split up and a gap at $k = \pi/2$ arises, as it is analytically shown in Giamarchi [31]. At $\delta = 1$ we get the peaks centered at $\omega = 0$ and $\omega = 2$, which corresponds to the conservation of $S^z_1 S^z_2$ at $\delta = 1$

and to the singlet- triplet gap, resp.[6]. The highest peak at $\delta = 1$ and $\omega = 0$ is a consequence of the degeneracy of the triplet ground state.

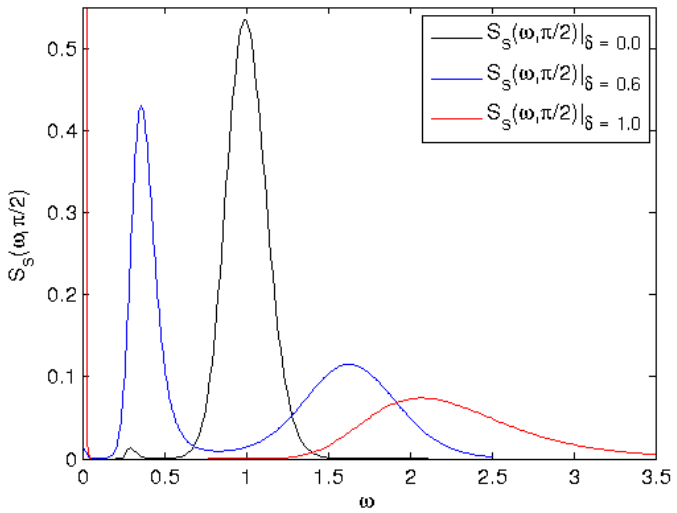

Figure 4.4: Spectral function evaluated from the $S^z S^z$ correlation, $J = -1$

In the following we show the spectral function in a two-dimensional momentum shade plot for every discrete $k \in [0, \pi]$ in one dimension and the energy ω in the second dimension for a demonstrative amount of δ-steps, see Fig. 4.5. The peaks of the spectral function of higher δ at low momentum k are quite small and therefore not all positions were marked.

The same procedure was done for an anisotropic Heisenberg model ($J_z = \frac{1}{2} J_{xy}, J = -1$) in Appendix B and for 'free fermions' ($J_z = 0, J = -1$) in Appendix C.

[6]The small peak of the $S_s(\omega, \pi/2)|_{\delta=0.0}$ spectral function at $\omega = 0.3$ is just an artifact, appearing after the 'Maximum Entropy' evaluation and is smaller than the errorbars (here neglected for better visualization)

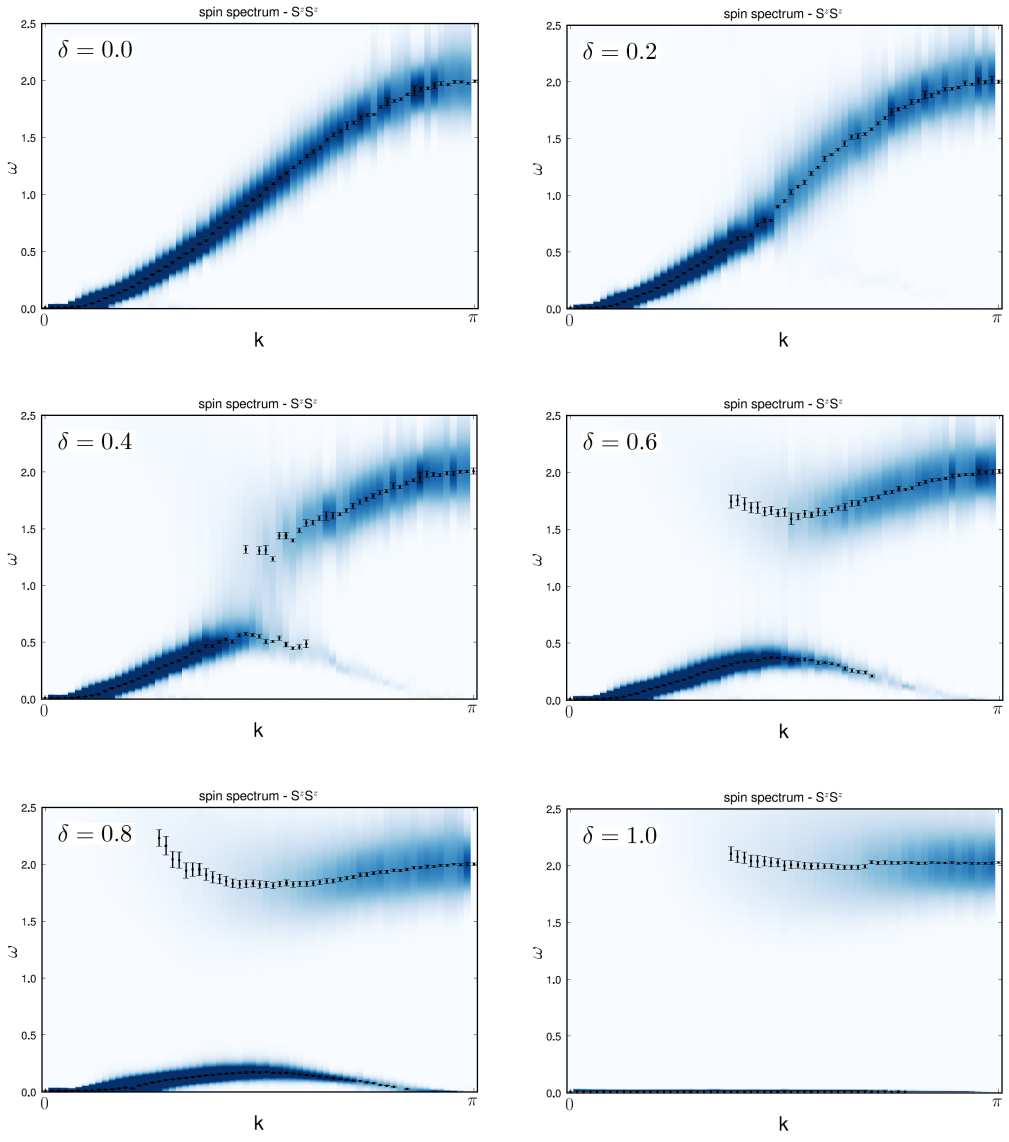

Figure 4.5: Shade plots of the spin S^zS^z spectral functions: $J = -1, L = 128$, $\beta = 32$

Chapter 5

Heisenberg chain with dynamic phonon interaction

5.1 Antiferromagnetic coupling

By treating the lattice classically with static phonon interaction (Chap. 4) we examined a Spin-Peierls Transition for the Heisenberg model. Now we start our consideration of the same model quantum mechanically with dynamic phonon interaction Eq. (2.8) with the following theorem:

Mermin-Wagner theorem [9]

Continuous symmetries cannot be spontaneously broken at finite temperature in systems with sufficiently short range interactions in dimensions $d \leq 2$.

Following the theorem, investigating the finite temperature case we do not expect a symmetry breaking. On the other hand, in the temperature limit $T \to 0$ a transition is expected for the AFM chain.
The thesis of Michel [2] investigated this system with quantum mechanically treatment of the lattice displacement. Suggested by Sandvik et al. [32] it is adequate to simulate a system with inverse temperature higher than $\beta = 2L$ [1], to obtain the zero temperature limit $(T \to 0)$[2]. The critical coupling can be determined by examining the staggered spin susceptibility Eq. (5.1).

[1] Increasing the inverse temperature does not appreciably change the spectral function $S(k, \omega)$ at all.

[2] For the following simulations the loop algorithm (see Evertz [18], Troyer et al. [33]) with local updates of the phonons was used.

$$\chi_S(\pi) = \frac{1}{L}\sum_{i,j}^{L}\int_0^\beta d\tau \left\langle S_i^z(\tau)S_j^z(0)\right\rangle \tag{5.1}$$

Following Okamoto et al. [34] the logarithmic correction of various variables vanishes at the critical coupling g_c. The staggered susceptibility, related to (see Sandvik et al. [32])

$$\chi_S(\pi) \sim L\ln^{\frac{1}{2}}\left(\frac{L}{L_0}\right) \tag{5.2}$$

can be plotted in a finite size scaling $(\chi_S(\pi)/L)^2$ vs. $\ln(L)$ for different coupling constants g_i. The curve will converge to a constant at the critical coupling g_c.
In the following, results from Michel [2] for the antiferromagnetic Heisenberg model with finite-frequency bond phonons (see Sec. 2.3 for the Hamiltonian) and at a bare frequency of the dispersion-less Einstein phonons $\omega_0 = 0.25$ are shown. The critical coupling was determined to be $g_c = 0.23(2)$.

The shade plot of the phonon spectral function Eq. (5.3), evaluated by measuring the phonon correlation $\langle x_{-k}(\tau)x_k(0)\rangle$ and by 'Maximum Entropy Theory', is shown in Fig. 5.1.

$$S_x(k,\omega) = \frac{1}{Z}\sum_{n,m} e^{-\beta E_n} |\left\langle m\right| x_k \left|n\right\rangle|^2 \delta(\omega - (E_m - E_n)) \tag{5.3}$$

At $g = 0.1 < g_c$ it exhibits a weak phonon branch, a so called central peak branch, close to $k = \pi$ and $\omega = 0$. It scales like $\omega(\pi) \to 0$ as $N \to \infty$. The inset demonstrates the distribution of the spectral weight and the blue shaded area illustrates the total spectral weight 0.5 of the non-interacting system. In this coupling regime the electron phonon branch preserves its spectral weight.

At the critical coupling g_c, Fig. 5.2, a softening of the electron phonon branch, caused by the spin phonon interaction can be recognized. Increasing the coupling causes a broadening of the peaks. Some spectral weight distributes to higher ω and the peak is no more located at the bare phonon $\omega_0 = 0.25$.

At higher coupling $g = 0.3 > g_c$ the renormalized bare phonons join the central peak branch and form a new single phonon branch in Fig. 5.3. Due

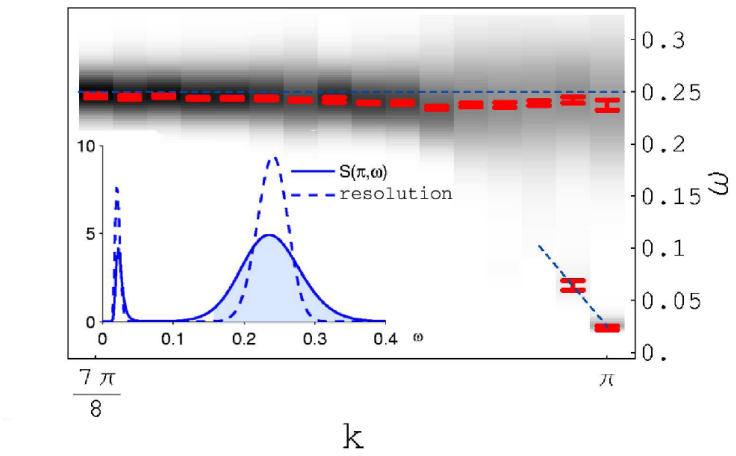

Figure 5.1: Shade plot of the phonon spectral function, $L = 256, \beta = 512, g = 0.1 < g_c$. A so called central peak branch, close to $k = \pi$ and $\omega = 0$, is shown. The inset shows the phonon spectral function $S_x(\pi, \omega)$, whereas the blue dotted curve indicates the resolution change, when using the momenta of the spectral function for the MaxEnt-evaluation (taken from the thesis of Michel [2]).

to the fact that for higher g calculations suffer from high autocorrelation a simulated tempering [35] was used.

For large ω_0 no softening of the phonons appears (see Michel [2]). The unaffected Einstein phonons and the central peak branch coexist beyond the phase transition.

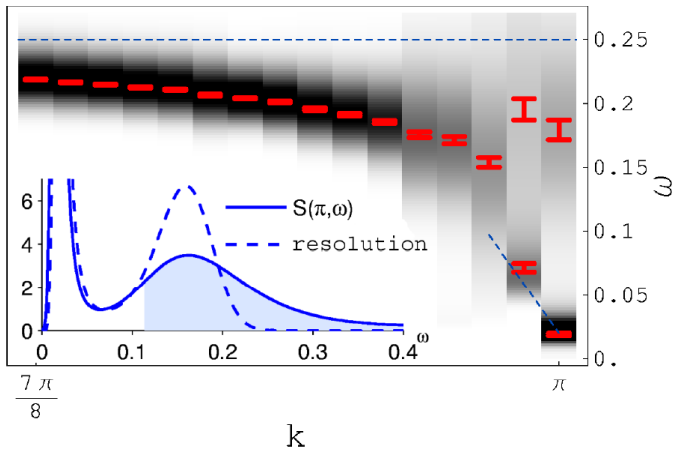

Figure 5.2: Shade plot of the phonon spectral function, $L = 256, \beta = 512, g = 0.23 \approx g_c$. A softening of the electron phonon branch, caused by the spin phonon interaction can be recognized. The inset shows the phonon spectral function $S_x(\pi, \omega)$, whereas the blue dotted curve indicates the resolution change, when using the momenta of the spectral function for the MaxEnt-evaluation (taken from the thesis of Michel [2]).

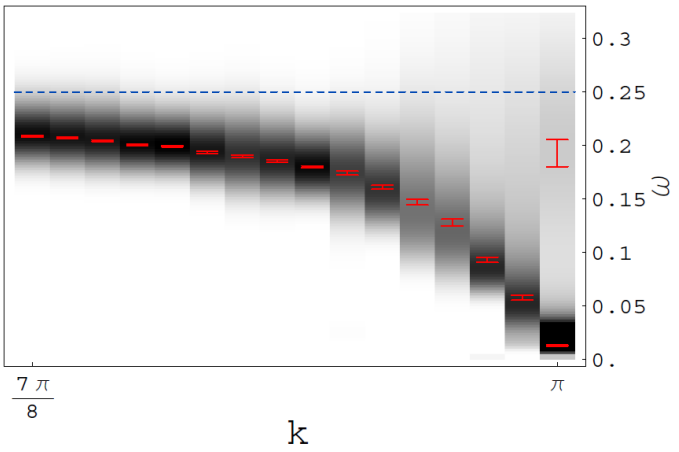

Figure 5.3: Shade plot of the phonon spectral function, $L = 256, \beta = 512, g = 0.3 > g_c$. The renormalized bare phonons join the central peak branch and form a new single phonon branch. The inset shows the phonon spectral function $S_x(\pi, \omega)$, whereas the blue dotted curve indicates the resolution change, when using the momenta of the spectral function for the MaxEnt-evaluation (taken from the thesis of Michel [2]).

5.2 Ferromagnetic coupling

Investigating the finite temperature case of ferromagnetic spin coupling a symmetry breaking is not expected at all, because of the Mermin-Wagner theorem. Calculations with the modified spin wave theory in the paper of Sirker et al. [4] estimated a gain in magnetic energy $E_{mag} \sim T^{3/2}$ for the static case, thus no SPT would occur in the $T \to 0$ limit.

We now examine the behavior of a small Heisenberg chain with fixed phonon states in an exact diagonalization and calculate the site energy E (Fig. 5.4 and Fig. 5.5), to get a feeling about the physical effects, when coupling and temperature change.

$$\hat{H} = \sum_{i=1}^{N} \left\{1 - g \cdot ((-1)^i x_i - (-1)^{i+1} x_i)\right\} \mathbf{S}_i^z \mathbf{S}_{i+1}^z \tag{5.4}$$

In Fig. 5.4 calculations for coupling constant $g = 0.25$ and different temperatures are shown. Decreasing the temperature a symmetry breaking becomes visible.

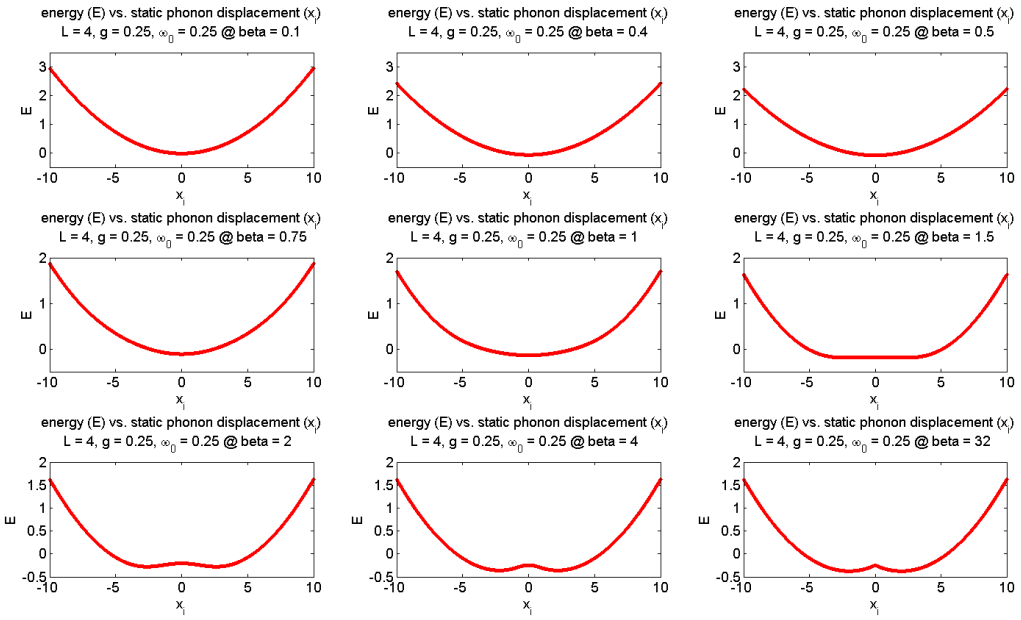

Figure 5.4: Site energy vs. phonon displacement of the Heisenberg chain with coupling constant $g = 0.25$

More clearly, for the stronger coupling constant $g = 0.5$ two minima for the total energy at higher temperatures can be seen, Fig. 5.5.

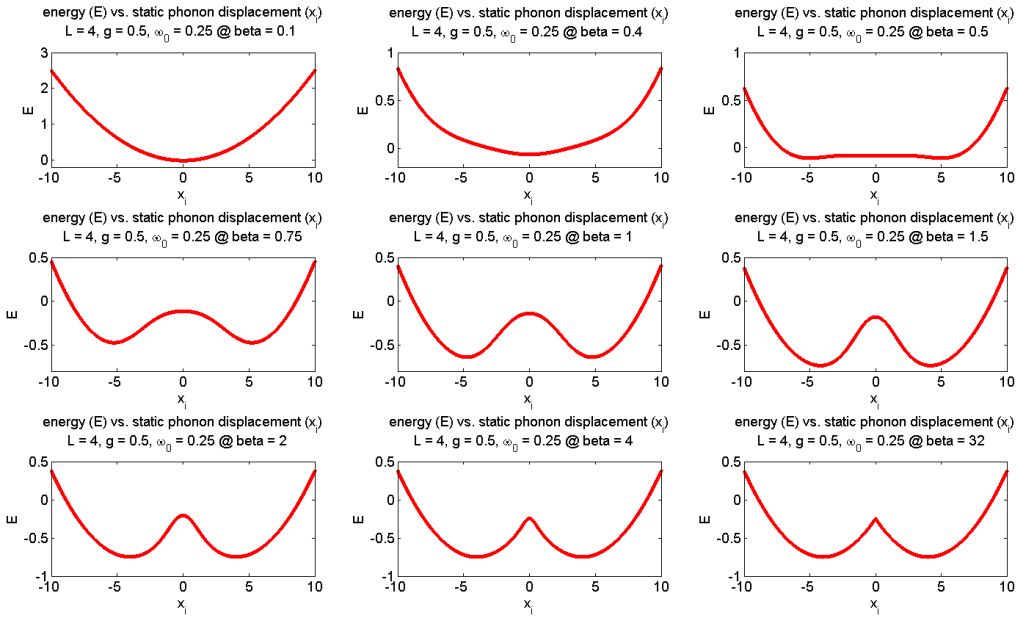

Figure 5.5: Site energy vs. phonon displacement of the Heisenberg chain with coupling constant $g = 0.5$

5.2.1 Mean Field Approximation for $T \to 0$

We treat the Hamiltonian Eq. (2.8) with the mean field approximation for energy calculation to obtain the dependence on the optical phonon energy ω and the phonon coupling constant g.
The energy E of a homogeneous ferromagnetic structure at low temperature contains the spin energy E_{spin} and the phonon energy E_{ph}.

$$E = E_{spin} + E_{ph} \simeq -(1 + g \cdot (x_i - x_{i+1})) \langle S_i S_{i+1} \rangle + \frac{\omega}{2} \tag{5.5}$$

If we consider the phonon displacement as small enough, we can approximate $(x_i - x_{i+1}) \to 0$ and get in terms of this for the energy $E = -\frac{1}{4} + \frac{\omega}{2}$.
We now demonstratively discuss a four spin chain with periodic boundary conditions. This leads to following four non-equivalent configurations and couplings:

$$\begin{aligned}
&\texttt{case 1}: \underbrace{\downarrow \ \downarrow \ \downarrow \ \downarrow}_{FM,FM,FM,FM} \\
&\texttt{case 2}: \underbrace{\downarrow \ \downarrow \ \downarrow \ \uparrow}_{FM,FM,AF,AF} \\
&\texttt{case 3}: \underbrace{\downarrow \ \downarrow \ \uparrow \ \uparrow}_{FM,AF,FM,AF} \\
&\texttt{case 4}: \underbrace{\downarrow \ \uparrow \ \downarrow \ \uparrow}_{AM,AF,AF,AF}
\end{aligned}$$

The FM/AF/FM behavior (case 3) is based on, in preliminary stages with QMC determined, simulation results. So after dimerization we propose and expect an alternating antiferromagnetic and ferromagnetic coupling between the spins. For the sake of completeness we also discuss case 1,2 and 4.
The site energy $\langle S_i S_{i+1} \rangle \approx \langle S_i \rangle \langle S_{i+1} \rangle$ is now systematically written like:

$$\langle S_i\rangle\langle S_{i+1}\rangle := A + (-1)^i B \tag{5.6}$$

$$\texttt{case 1} : \langle S_i\rangle\langle S_{i+1}\rangle = \left\{\frac{1}{4}, \frac{1}{4}, \frac{1}{4}, \frac{1}{4}\right\} \widehat{=} \frac{1}{4} + (-1)^i 0 \tag{5.7}$$

$$\texttt{case 2} : \langle S_i\rangle\langle S_{i+1}\rangle = \left\{\frac{1}{4}, \frac{1}{4}, -\frac{1}{4}, -\frac{1}{4}\right\} \tag{5.8}$$

$$\texttt{case 3} : \langle S_i\rangle\langle S_{i+1}\rangle = \left\{\frac{1}{4}, -\frac{1}{4}, \frac{1}{4}, -\frac{1}{4}\right\} \widehat{=} 0 + (-1)^i \frac{1}{4} \tag{5.9}$$

$$\texttt{case 4} : \langle S_i\rangle\langle S_{i+1}\rangle = \left\{-\frac{1}{4}, -\frac{1}{4}, -\frac{1}{4}, -\frac{1}{4}\right\} \widehat{=} -\frac{1}{4} + (-1)^i 0 \tag{5.10}$$

The phonon displacement x_i couples to energies in the following way,

$$\langle S_i S_{i+1}\rangle - \langle S_{i+1} S_{i+2}\rangle = \begin{cases} 2B & \text{i : } \texttt{even} \\ -2B & \text{i : } \texttt{odd} \end{cases} \tag{5.11}$$

or shows for configuration case 2 following behavior:

$$\langle S_i S_{i+1}\rangle - \langle S_{i+1} S_{i+2}\rangle = \begin{cases} 0 & \text{i : } \texttt{even} \\ \frac{1}{2} & \text{i : } \texttt{odd} \end{cases} \tag{5.12}$$

Therefore we can write the phonon Hamiltonian:

$$\begin{aligned} \hat{H}_{i_{ph}} &= \frac{\hat{p}_i^2}{2m} + \frac{\omega^2}{2} x_i^2 \pm 2gBx_i \\ &= \frac{\omega^2}{2} \underbrace{\left(x_i \pm \frac{2Bg}{\omega^2}\right)^2}_{\tilde{x}_i^2} - \underbrace{\frac{\omega^2}{2}\left(\frac{2gB}{\omega^2}\right)^2}_{\Delta E_{ph}} \end{aligned} \tag{5.13}$$

Neglecting the kinetic part and separating the energy gain ΔE_{ph} by completing the square structure.

$$\Delta E_{ph} = \frac{2g^2B^2}{\omega^2} \tag{5.14}$$

For the configuration cases 1 and 4 no gain in elastic energy ΔE_{ph}, because of $B = 0$ and Eq. (5.11), appears.

With alternating AF/FM couplings (case 3) we can estimate:

$$2g|\Delta x_i| = \frac{2|g|^2}{\omega^2} \underbrace{2B}_{=\frac{1}{2}} \tag{5.15}$$

Neglecting the phonon part, for the FM state we get for the spin energy:

$$E_{spin}^{FM} = -\frac{1}{4} \tag{5.16}$$

Considering the case differentiation Eq. (5.12) and Eq. (5.13) for configuration case 2 a gain in elastic energy ΔE_{ph} can be determined.
In the dimerized case (case 3) we can estimate for the spin energy:

$$\begin{aligned} E_{spin}^{D} &= -\frac{1}{2}\left[(1+g\underbrace{(x_i - x_{i+1})}_{\to 0})\frac{1}{4} + (1+g\underbrace{(x_i - x_{i+1})}_{\to 0})\left(-\frac{1}{4}\right)\right] \\ &= -\frac{1}{2}\left[\frac{1}{4} - \frac{1}{4}\right] = 0 \end{aligned} \tag{5.17}$$

The energy difference between E_{spin}^{FM} and E_{spin}^{D} will be $\frac{1}{4}$ and causes a total energy gain and an expected Peierls transition at low temperature ($T \to 0$) if:

$$\frac{1}{4} < \frac{2g^2B^2}{\omega^2} \underbrace{\Longleftrightarrow}_{B=\frac{1}{4}} \underline{\underline{|g| \geq 2|\omega|}} \tag{5.18}$$

Note: An other ansatz showed that this relation between the coupling constant g and phonon energy ω might be too high and the Spin-Peierls transition will already occur at $|g| \geq |\omega|$ for low temperatures.

5.3 No Spin-Peierls Transition in one dimension with ferromagnetic coupling

Fig. 5.6 and Fig. 5.7 show phonon correlations $\langle x_0 x_j \rangle$ of QMC simulation of a Heisenberg FM chain ($L = 16$) with dynamic site phonons at different temperature- and phonon coupling regimes[3]. No correlation can be seen, therefore the system is not dimerized, as consequence: No Spin-Peierls Transition occurs as expected.

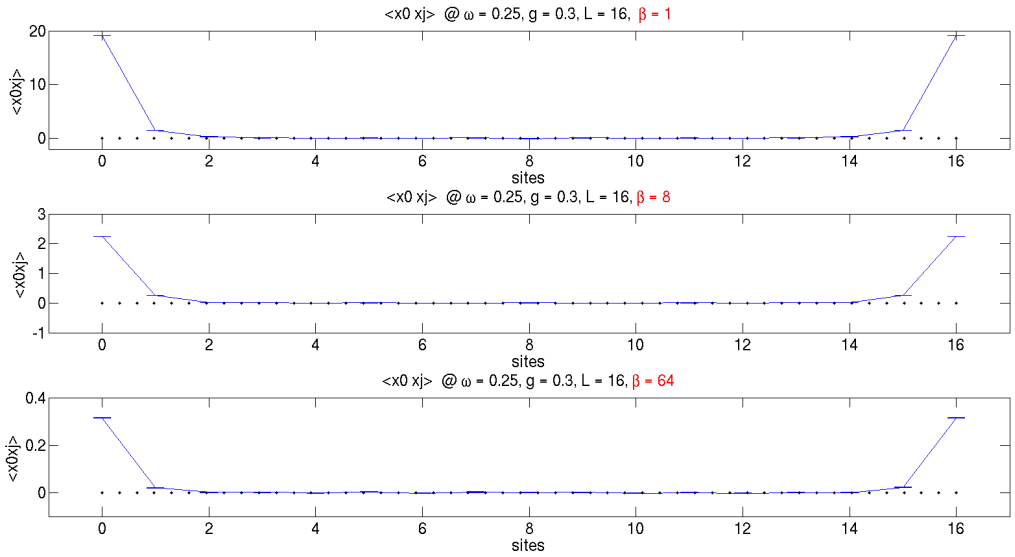

Figure 5.6: Phonon correlation $\langle x_0 x_j \rangle$ for different inverse temperatures β. Within a few sites the correlation is tending to zero.

This is also evident when considering the phonon correlation function $\langle x(\tau)x(0) \rangle$ at $k = \frac{\pi}{2}$ Fig. 5.8, where a Spin-Peierls Transition might occur. The correlations at the phonon coupling constants $g = 0$ and $g = 0.3$[4] are compared to the analytic solution for $g = 0$[5]. No differences in the energy spectrum can be observed, so no indication for a phase transition can be seen.

[3] For the simulations $L \cdot 10^5$ sweeps were used (10% for thermalization).

[4] This is chosen to be higher than the critical coupling g_c estimated in the static case.

[5] $\langle x(\tau)x(0) \rangle = \frac{\omega(k)}{\omega(k)^2 + \omega_n^2}$ evaluated from Eq. (3.39) and Eq. (3.62)

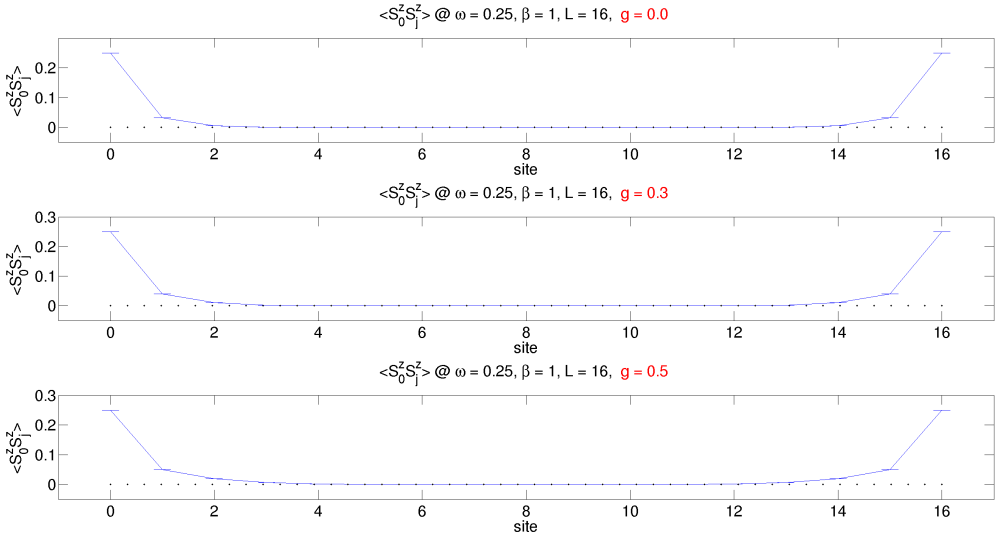

Figure 5.7: Phonon correlation $\langle x_0 x_j \rangle$ for different phonon couplings g. Within a few sites the correlation is tending to zero.

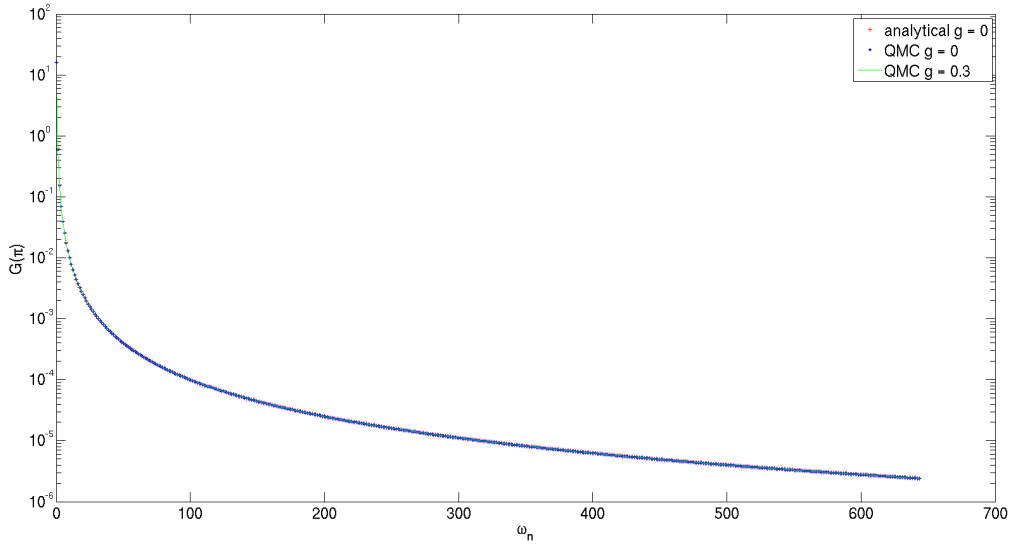

Figure 5.8: Comparison of the phonon Green's functions $\langle x(\tau)x(0)\rangle_{\pi/2}$ for $g = 0$ and for $g = 0.3$ with an analytically solution for $g = 0$. $L = 16$ and $\beta = 5$

Chapter 6

Coupled Heisenberg chains with static phonon interaction

In this Chapter we investigate the Hamiltonian H_{spin} of Sec. 2.5. We take Heisenberg chains with periodic static phonons and couple them with a strong perpendicular magnetic inter-chain coupling constant, of the same size as the parallel spin coupling constant $J_\perp = J_\parallel = -1$, to get the best guaranty for the two-dimensional behavior of a quantum system[1].
In contrast to the one-dimensional ferromagnetic Heisenberg model with static phonon interaction (see e.g. Sirker et al. [4]) we do not have any predictions for the two-dimensional model and its behavior.
In the following, QMC simulations with periodic static phonons (Sec. 3.3) of a two-dimensional system with length $L = 64$, width $W = 64$ and inverse temperature $\beta = 32$ for a demonstrative amount of phonon displacements δ are determined[2]. Fig. 6.1 shows the spectral functions in a two-dimensional shade plot for every discrete momentum k and the energy ω. At $\delta \geq 0.6$ it shows the rising energy gap at $k = (\pi/2, 0)$ and $k = (\pi/2, \pi/2)$, caused by a magnetic energy gain from distorting the lattice with a displacement δ. The spin S^zS^z correlation (Green's function Sec. 3.8) of the two-dimensional system was measured and the spectral function $S(\omega)$ determined[3] by using the 'Maximum Entropy technique', Sec. 3.8.2.

In the adiabatic approximation of the phonons, we again consider the

[1] We too choose length and width of same size $L = W$ for the simulations.

[2] For the simulations $L \cdot 10^5$ sweeps were used (10% for thermalization).

[3] There are different ways of arranging spectral functions in the shade plot. Here, in two-dimensional reciprocal space, we have chosen the following way to go through the lattice: We start at $k = (0, 0) \rightarrow k = (\pi, \pi)$, from here to $k = (\pi, \pi) \rightarrow k = (\pi, 0)$, back to the beginning $k = (\pi, 0) \rightarrow k = (0, 0)$.

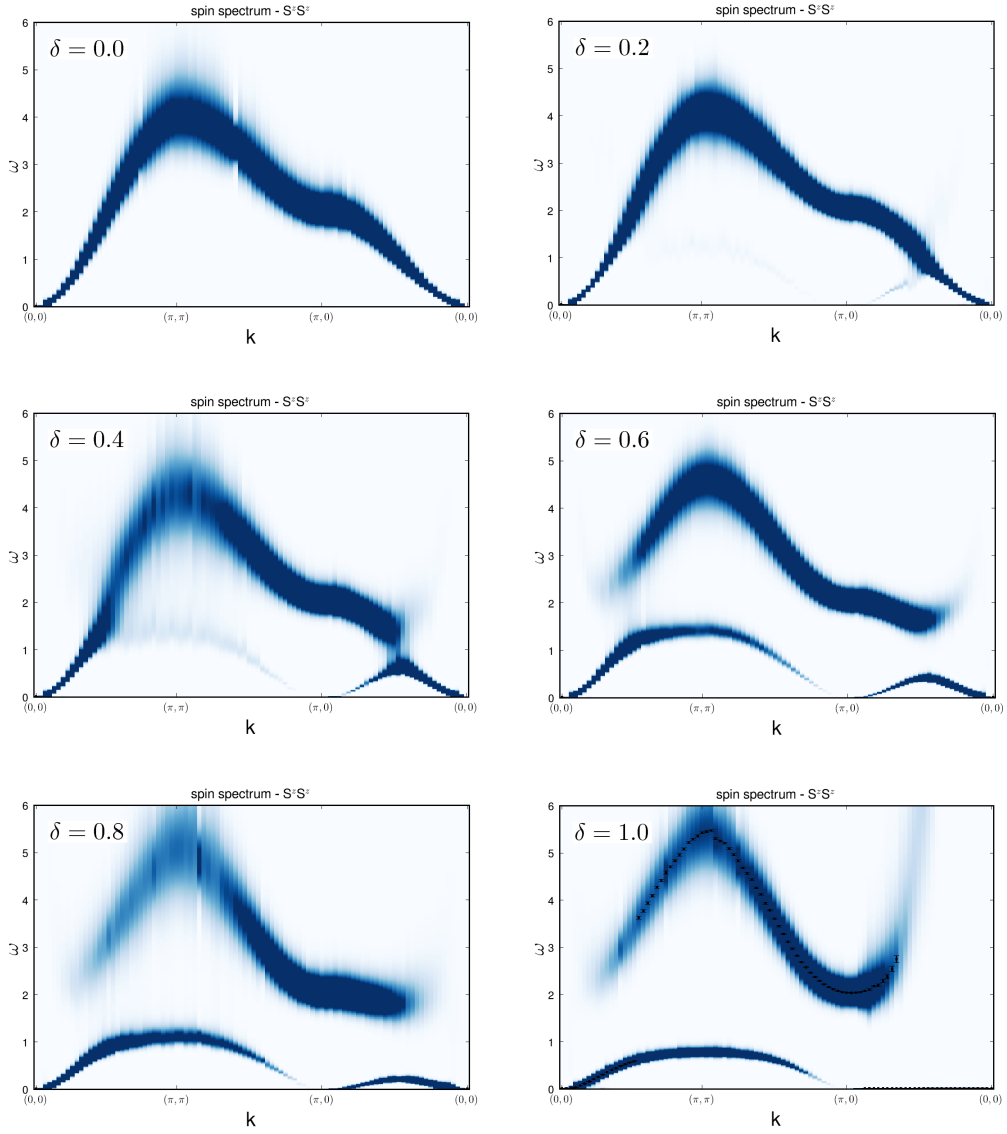

Figure 6.1: Shade plot of the spin S^zS^z spectral function: $L = 64, W = 64$, $\beta = 32$

Hamiltonian $H = H_{spin} + E_{el}$. Competing to a possible gain in magnetic energy $E_{spin}(\delta = 0 \rightarrow 1)$ there is the cost in elastic energy $E_{el} = K\delta^2/2$ per site, with K the effective elastic constant.
In Fig. 6.2 the spin energy E_{spin} per site of different inverse temperatures β vs. δ^2 are plotted. To get a feeling for the finite size behavior the calculations were done for several system sizes.

For the ground state with the ferromagnetic coupling ($\beta \to \infty$), as indicated[4] in Fig. 6.2 no gain in magnetic energy will occur. Even for any value of phonon displacement $\delta \in [0, 1]$ the system will stay in the fully polarized FM state.

For higher temperature there is again a significant energy gain between $E_{spin}(\delta = 0)$ and $E_{spin}(\delta \to 1)$, similar to the purely one-dimensional case. Thus there appears to be a Peierls transition with static phonons in the two-dimensional case as well.

[4]Because of computational efforts for $\beta = 96$ a non-quadratic lattice (24x6) was chosen.

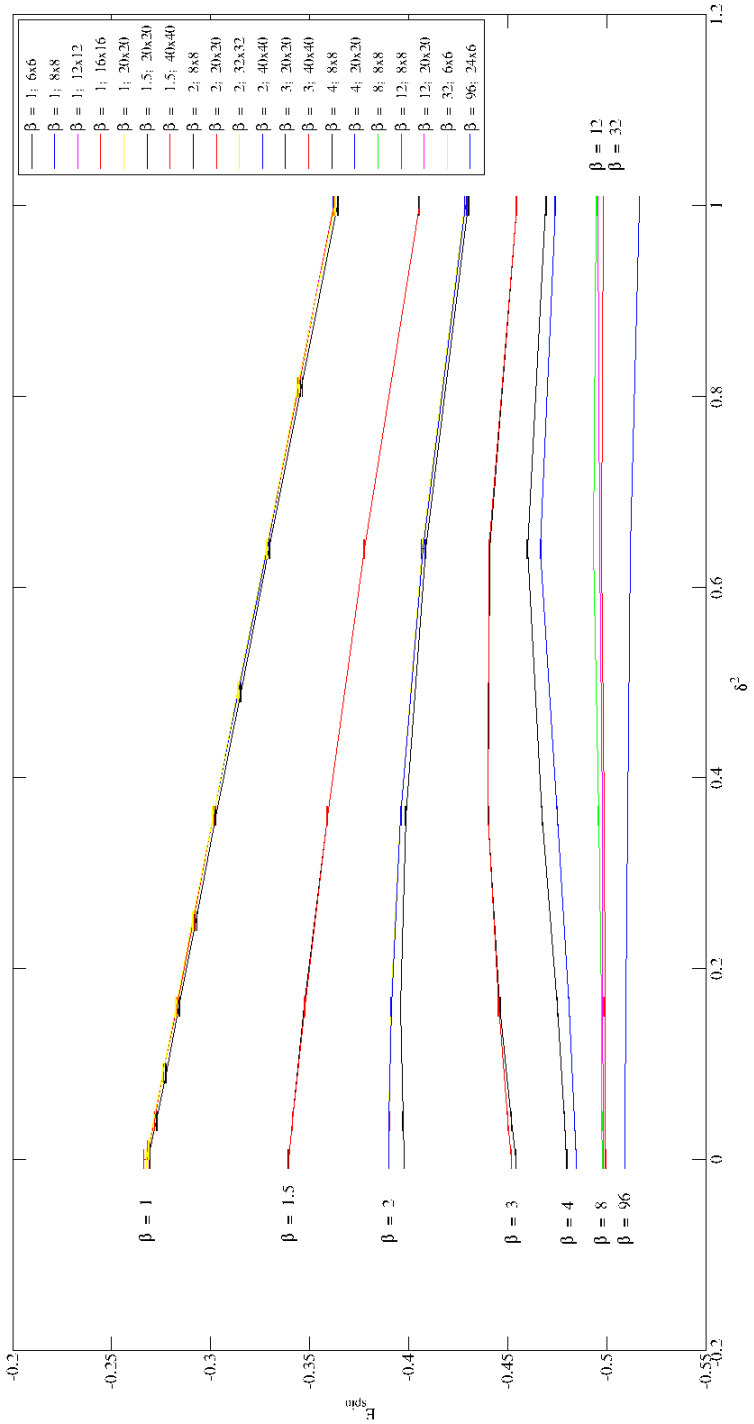

Figure 6.2: Spin energy E_{spin} vs. δ^2 for different inverse temperatures β and system sizes

Chapter 7

Coupled chains with dynamic phonon interaction

7.1 Antiferromagnetic coupling

The simulations of coupled Heisenberg chains with dynamic bond phonons, shown here, are based on a realistic description of e.g. $CuGeO_3$, see Sec. 2.6, with an estimated weak intra-chain coupling constant $J_\perp = 0.1$ and bare phonons with $\omega_0 = 0.25$. Investigating this model in the static phonon case a magnetic energy gain $E_{mag} \sim \delta^2$ of the same order as the lattice distortion energy E_{el} can be ascertained, see Sirker et al. [36][1]. Considering the temperature limit $T \to 0$, it is sufficient to choose the inverse temperature $\beta = 4L$ as described in Uhrig et al. [37].

The staggered spin susceptibility $\chi(\pi, \pi)$ Eq. (7.1) scales as $\chi(L) \sim L^{2-\eta}$ (critical exponent $\eta = 0.0375(5)$ from [38]).

$$\chi_S(\pi,\pi) = \frac{1}{L\beta} \sum_{i,j} \sum_{i',j'} \int_0^\beta d\tau (-1)^{i-i'+j-j'} \left\langle S^z_{i,j}(\tau) S^z_{i',j'}(0) \right\rangle \qquad (7.1)$$

Plotting $\chi(L)/L^{2-\eta}$ vs. coupling g for different system sizes, the critical coupling g_c can be evaluated from the intersection point of these curves[2]. The critical coupling has been determined as $g_c = 0.45(1)$, see Michel [2].

[1] The critical coupling g_c for finite lattice distortion will be higher than it is in the one-dimensional case.

[2] shown in Favorsky et al. [39]

In the shade plot of the phonon spectral function Fig. 7.1 a softening of the $(k_x, 0)$-phonon branch at $g = 0.425$ near the critical coupling g_c can be seen[3]. We expect only one branch, because the phonons couple only in one dimension. Here a system with $L = 40$ and $W = 10$ is displayed. In Michel [2] its two-dimensional behavior with the ration $R = L/W = 4$ was shown.

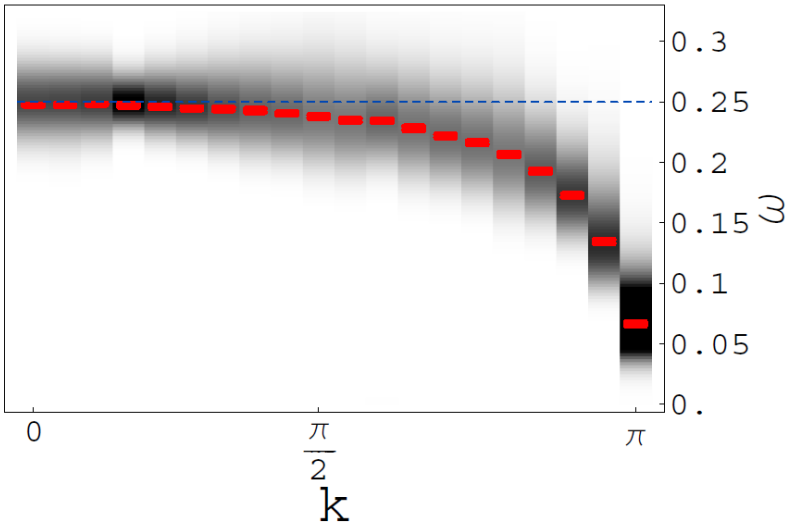

Figure 7.1: Shade plot of the phonon spectral function,
$L = 40, W = 10, \beta = 160, g = 0.425$, evaluated in $k = (k_x, 0)$ direction (taken from the thesis of Michel [2])

Contrary to the predictions of QMC simulations of classical elastic lattices of Sengupta [40], the Spin-Peierls phase transition seems to be of second order, see Michel [2].

[3]For this simulation the loop algorithm (see Evertz [18]) with global spin updates and local updates of the phonons were used. For large couplings g a simulated tempering has to be implemented, because the updates suffer from high autocorrelations, see Michel [2]. At least 10^5 sweeps were sampled and 10% skipped for thermalization.

7.2 Ferromagnetic coupling

We now implement a ferromagnetic coupling in our two-dimensional Heisenberg model with dynamic site phonon interaction in one dimension. Because of our investigation in the static case Fig. 6.2 we expect a possible Spin-Peierls transition in the higher temperature case $\beta \sim 1.5$. To ensure a two-dimensional behavior of the system a strong intra chain coupling $J_\perp = -1$ and a squared lattice $L = W$ is chosen. In Fig. 7.2 a snapshot of the next nearest phonon displacements $(x_i - x_{i+1})$ vs. imaginary time τ is illustrated. A staggered inter- and intra chain correlation is recognizable.

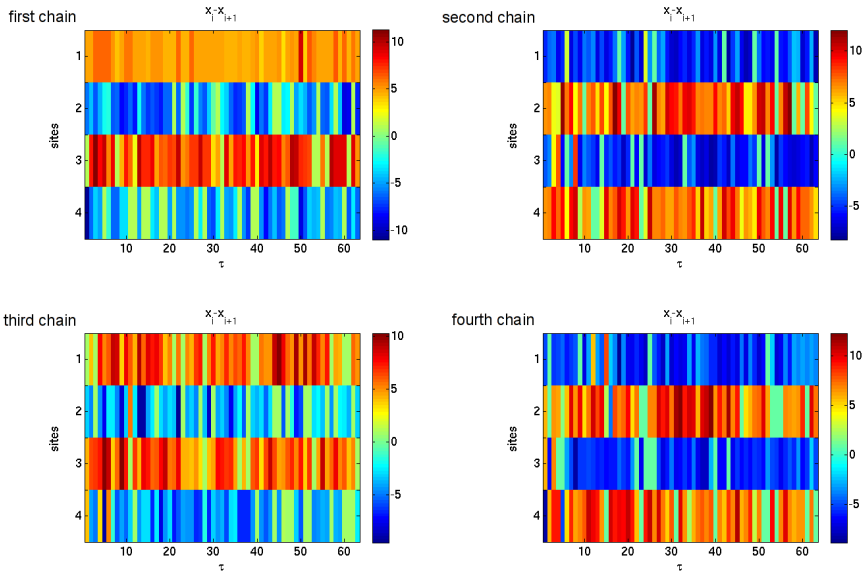

Figure 7.2: These four snapshots illustrate the differences of the next nearest phonon displacements $(x_i - x_{i+1})$ of a 4x4 lattice with $g = 0.5$ and $\beta = 1$. The sites of a chain are plotted versus the imaginary time τ. The phonon displacements are well correlated to each other, in intra- as well as in inter chain dimension.

We now treat the model in a 'Mean Field Approximation' to evaluate an approximate critical spin phonon coupling g_c.

7.2.1 Mean Field Approximation

First we expand our ansatz for the spin energy E_{spin} up to the 4^{th} power of δ.

$$E_{spin} = a - b\delta^2 - c\delta^4 \tag{7.2}$$

The phonon energy E_{ph} is written as the potential part,

$$E_{ph} = \frac{k}{2}x^2 \tag{7.3}$$

with the following relation between ω and k

$$\omega^2 = \frac{k}{m} = k \tag{7.4}$$

The estimator of the Hamiltonian is rewritten in the mean field treatment. The phonon coupling g and displacement x is set in relation to the static phonon displacement δ. Thereby we can fit our parameters with the calculations of the previous section (Fig. 6.2).

$$\begin{aligned}\langle H\rangle &= \langle (1+gx)SS + \frac{k}{2}x^2\rangle \\ &\simeq (1+\underbrace{g\langle x\rangle}_{\pm\delta})\langle SS\rangle + \frac{k}{2}\langle x\rangle^2\end{aligned} \tag{7.5}$$

Changing the phonon energy E_{ph} to static displacement δ notation

$$E_{ph} = \frac{k}{2g^2}\delta^2 \tag{7.6}$$

we get for the total energy E:

$$E = a - b\delta^2 - c\delta^4 + \frac{k}{2g^2}\delta^2 \tag{7.7}$$

In the limit $\delta \to 0$ and $\delta \to 1$ we obtain:

$$E(\delta = 0) = a \tag{7.8}$$
$$E(\delta = 1) = a - b - c + \frac{k}{2g^2}$$

In case of low inverse temperature β, a gain in magnetic energy (lowering of $E_{spin}(\delta \to 1)$) can be determined from of Fig. 6.2. We can carry on our consideration to get an approximation of the magnitude of the phonon critical coupling constant g_c, where dimerization should appear.

$$E(\delta = 1) < E(\delta = 0) \to \frac{k}{2g^2} < b + c$$

$$k = \omega^2$$

$$g^2 > \frac{\omega^2}{2(b+c)}$$

In a least square approximation we fit the spin energy E_{spin} vs. δ^2 of the static case (Fig. 6.2) for a certain inverse temperature $\beta = 1.5$[4] (Fig. 7.3) and get the following coefficients[5]: $a = -0.390, b = 0.004, c = 0.034$.

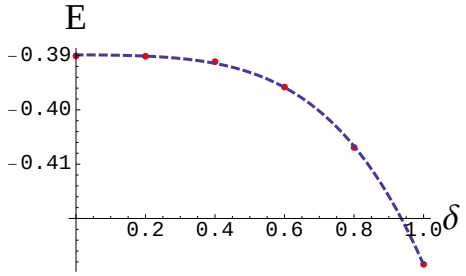

Figure 7.3: Spin energy vs. δ. The blue dashed curve is a least square fit of the energy expectation value (red points)

With the fixed Einstein phonon energy $\omega_0 = 0.25$ we should therefore get dimerization at $g_c \approx 0.90$.

[4]At this inverse temperature we get a noticeable gain of magnetic energy and the temperature is still low enough not to smear out the correlations shown later.

[5]The errors of the least square approximation are therefore not important at all.

7.2.2 Spin-Peierls Transition in two dimensions with ferromagnetic coupling

In simulations of the two-dimensional ferromagnetic coupled Heisenberg chains at $\beta = 1.5$ we observe anti-correlated phonon states $\langle x_0 x_j \rangle$ as a function of the sites of the first chain, see Fig. 7.4. Unfortunately the mean values of the phonon displacements are far away from their exact expectation value of zero at large g. This implies that autocorrelations are large and improved simulation techniques like tempering should be employed. Still, the correlations $\langle x_0 x_j \rangle$ should only be affected by autocorrelations to a much smaller degree than $\langle x_i \rangle$. Therefore the observed staggered values of $\langle x_0 x_j \rangle$ in Fig. 7.4 provide a strong motivation of a dimerized phase.

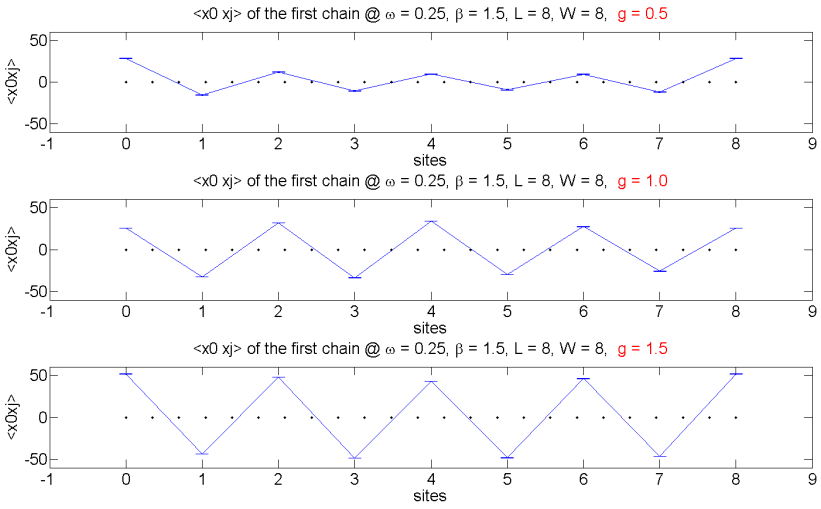

Figure 7.4: Phonon correlation $\langle x_0 x_j \rangle$ of the first chain for different couplings g

Having a closer look at the values of the anti-correlated phonon states we see that they imply an alternating intra-chain FM/AM-coupling. The same behavior can be seen in the second dimension, although the displacements are of different heights, which also indicates lack of full convergence. In Fig. 7.5 the $\langle S_0^z S_j^z \rangle$ correlation is plotted. For low coupling g the correlation approaches zero within a few sites. This behavior was already shown at $g = 0$ by Favorsky et al. [39]. Contrary to this, the spin correlation does not vanish for higher coupling g. That means the spins become correlated at large distances.

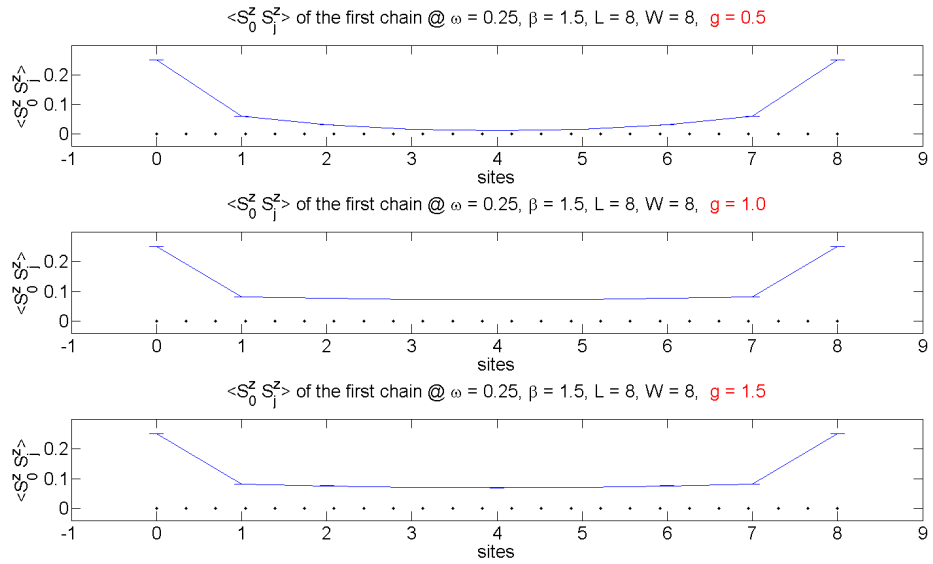

Figure 7.5: Spin correlation $\langle S_0^z S_j^z \rangle$ of the first chain for different couplings g

Some simulations were performed with tempering. The results for the site energy $\langle S_i S_{i+1} \rangle$ are shown in Fig. 7.6[6]. The energy begins to rise sharply at a coupling of $g = 0.8$, indicating a phase transition at this coupling. Thus the simulations of the two-dimensional ferromagnet with dynamic site phonons indeed show that the system very likely has a Spin-Peierls transition to a dimerized phase at finite phonon coupling g.

[6]Simulations of few coupling constants and with insufficient 640.000 sweeps (100.000 thermalization) were done, because of technical problems, see Sec. 3.6.

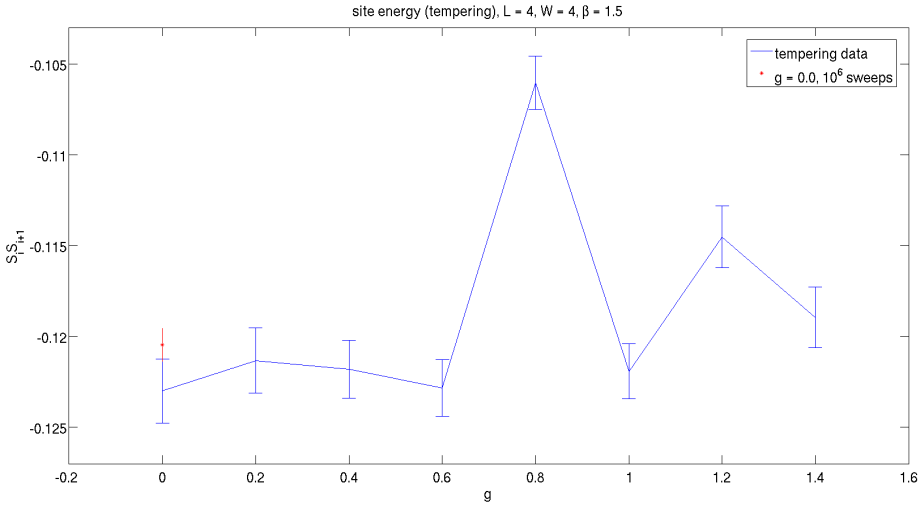

Figure 7.6: Site energy $\langle S_i S_{i+1} \rangle$ vs. phonon coupling g, $L = 4, W = 4$, $\beta = 1.5$. Although tempering was used for this evaluation, the system is at large g not converged at all. Nonetheless, because of significant change of the site energy a possible phase transition can be seen qualitatively around $g = 0.8$. As a benchmark for the tempering data, a simulation with $g = 0.0$ is shown with net 10^6 sweeps (red point with errorbar).

Chapter 8

Overall conclusions

In this thesis we have studied the one- and two-dimensional spin-1/2 Heisenberg model coupled to static (classic lattice displacement) and dynamic phonons (quantum mechanical description of lattice degrees of freedom). This model is motivated by materials like the quasi one-dimensional Bechgaard-salt, showing an experimentally measurable structural quantum phase transition, the so called Spin-Peierls Transition (SPT).

The investigations of the different Heisenberg models with phonons have been performed by Quantum Monte-Carlo (QMC) simulations, treating the partition function in a Stochastic Series Expansion (SSE). The lattice degrees of freedom have been introduced in the so called interaction representation. A Fast Fourier Transform, which costs most of the computational effort, transforms the configurations to momentum and frequency space in which new phonon configurations can be sampled efficiently. The spins are updated via a directed loop algorithm. Via this algorithms site and bond phonons and any bare phonon dispersion can be implemented. This thesis is restricted to discussions of dispersion-less optical phonons.

Based on work by J. Sirker for static phonon interactions we studied the ferromagnetic Heisenberg model in one dimension which has a phase transition at finite temperature, determined the spectra of spin excitations, the spin order parameter and the energy versus phonon dispersion at finite temperatures.
For dynamic phonons in one dimension, the Mermin-Wagner theorem states that a phase transition can only take place at $T = 0$. In the antiferromagnetic chain such a transition takes place at finite coupling g, and spectra from F. Michel [2] were shown for comparison. While a mean field calculation would indicate a transition, we verified by QMC calculations that instead no dimer-

ization occurs in the phonon coordinates.
We then investigated two-dimensional systems of coupled chains, with phonon coupling along the chains. For static phonons and ferromagnetic spin coupling we calculated the spin spectra by QMC and determined the spin energy as a function of phonon displacement δ at different temperatures, finding that there is an energy gain at large T, similar to the one-dimensional case.
With dynamic phonons it is known for AF coupling from Michel [2] that there is a zero-temperature phase transition. We investigated the FM case and estimated the critical coupling in a Mean Field calculation and obtained an estimated critical coupling of $g \approx 0.9$ at an inverse temperature of $\beta = 1.5$.
Finally we performed QMC calculations with dynamic phonons, which turned out to suffer from large autocorrelations at large g. Still they showed very strong indication that there is indeed a phase transition to a dimerized phase for the two-dimensional FM Heisenberg model at finite temperature.
Further simulations should follow to improve convergence and to drastically reduce autocorrelations.

This following table represents a short overview of Spin-Peierls Transitions:

1d *static* phonons:	
antiferromagnetic chain	always dimerized
ferromagnetic chain	transition at finite T
1d *dynamic* phonons:	
antiferromagnetic chain	SPT at zero T and $g > g_c$
ferromagnetic chain	NO dimerization
2d *static* phonons:	
antiferromagnetic coupled chains	always dimerized
ferromagnetic coupled chains	transition at $T > 0$
2d *dynamic* phonons:	
antiferromagnetic coupled chains	$T > 0$ not investigated
ferromagnetic coupled chains	transition at $T > 0$

Appendix A

Spin-1-Heisenberg chain

The behavior of the order parameter for a spin-1-Heisenberg FM with static phonon interaction[1] is shown in Fig. A.1.

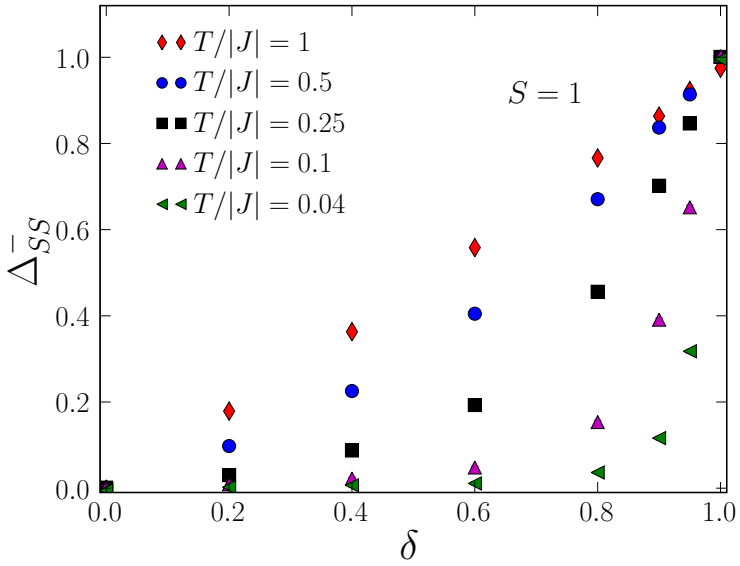

Figure A.1: Spin order parameter Δ^{-}_{SS} for Spin 1, $J = -1, L = 128$, errorbars are smaller than the symbols

At lower temperature behavior the order parameter rises in a sharper way than for the spin-1/2 system to the asymptotic energy. Also here in case of Spin-1 the highest temperature spin order parameter $T = 1$ for $\delta = 1$ is, because of higher excitations, less than the asymptotic FM energy $E = 1.0$.

[1] This was also calculated by Sirker *et al.* [4] with TMRG and should be seen as a cross-check for our SSE-QMC. The results of TMRG and QMC are identical.

Appendix B

Anisotropic FM

In Fig. B.1 we can see the site energy related to the static phonon displacement δ coupled to an anisotropic FM model ($J_z = 1/2 J_{xy}, J_{xy} = -1$) at high inverse temperature $\beta = 32$. Different from the results of the Heisenberg chain Fig. 4.3 an energy gain at higher displacement is clearly visible.

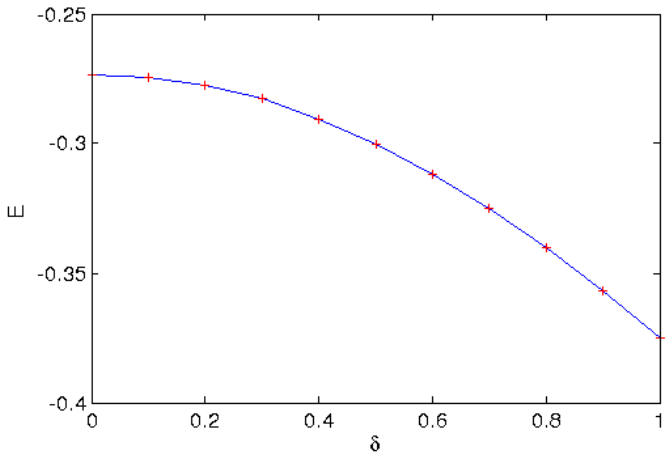

Figure B.1: Site energy E of the anisotropic FM model vs. static phonon displacement $\delta, J_z = \frac{1}{2} J_{xy}, J_{xy} = -1, \beta = 32, L = 128, \Delta E = 10^{-4}$

In Fig. B.2 the spectral function $S_s(\omega, \pi/2)$ is shown. Only a single peak arises, centered around the singlet energy at higher static phonon displacement ($\delta \to 1$).

In Fig. B.3 the spectral functions are shown in the two-dimensional shade plot for several static phonon displacements δ. Calculations of the anisotropic FM model without static phonon interaction were done in Sugiyama [41]. The

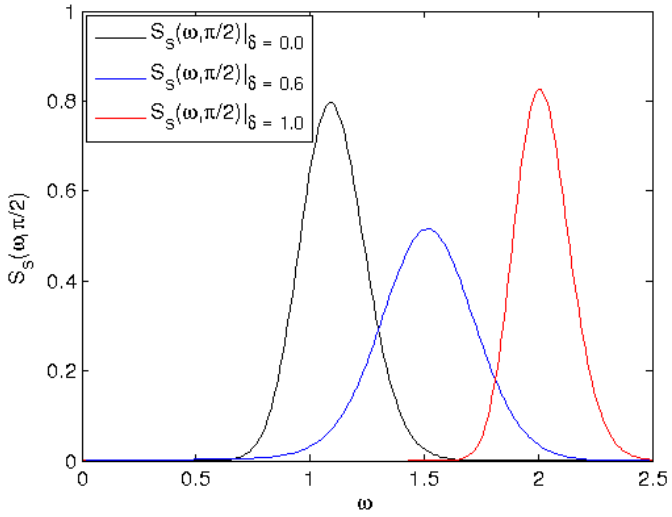

Figure B.2: Spectral function evaluated from the S^zS^z correlation, $J_{xy} = -1$, $J_z = \frac{1}{2}J_{xy}$

peak close to $\omega = 0$ in Fig. 4.4, 4.5 is not present, since the ground state is unique here.

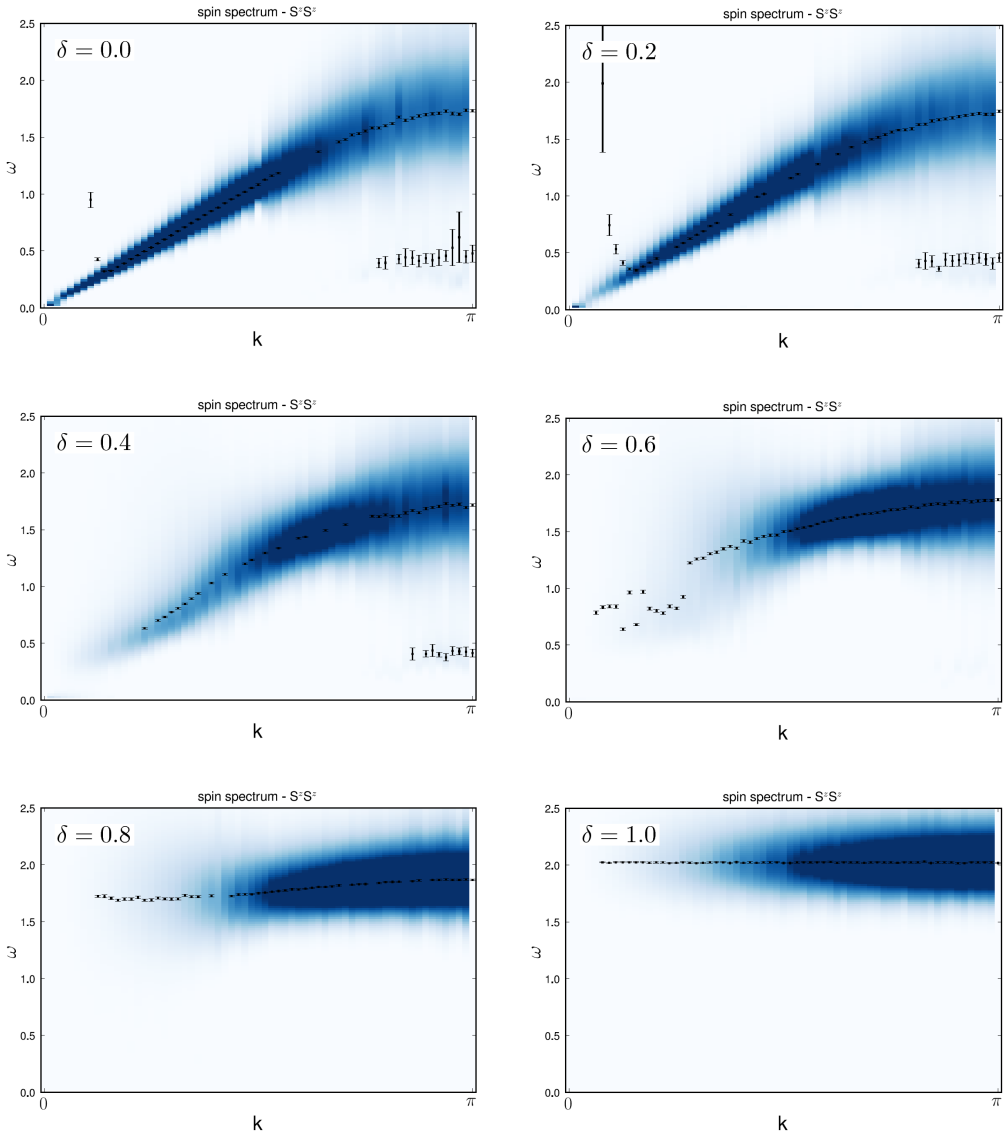

Figure B.3: Shade plots of the spin S^zS^z spectral functions: $J_{xy} = -1$, $J_z = \frac{1}{2}J_{xy}, L = 128, \beta = 32$

Appendix C

Free fermions

In Fig. C.1 the site energy of the free fermion model ($J_z = 0, J = -1$) with static phonon displacement δ at high inverse temperature $\beta = 32$ is shown. Similar to Fig. B.1 an energy gain towards higher displacement is in this temperature regime clearly visible.

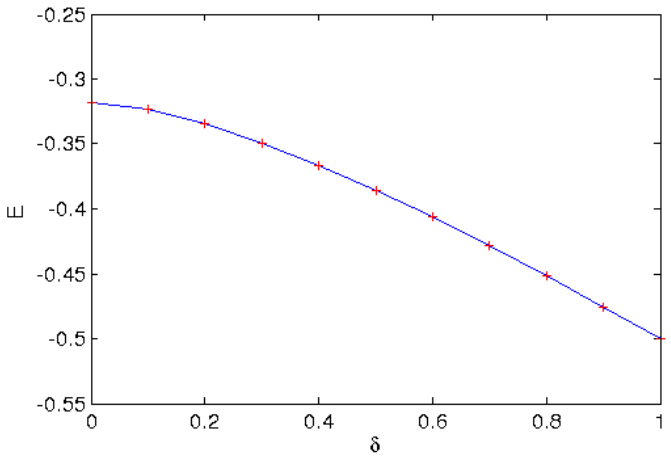

Figure C.1: Site energy E of the free fermion model vs. static phonon displacement $\delta, J_z = 0, J_{xy} = -1, \beta = 32, L = 128, \Delta E = 10^{-4}$

The spectral function $S_s(\omega, \pi/2)$ for several static phonon displacements δ is shown in Fig. C.2.

The dispersion relation of the free fermion model, see Fig. C.3 is cross-calculated by 'Time Evolving Block Decimation Algorithm (TEBD)' [1].

[1] by a colleague 'Elias Rabel' in the course of his diploma thesis 'Numerical Time Evolution of 1D Quantum Systems' [42] compared to Fig. C.4 and the paper of Gouvea et

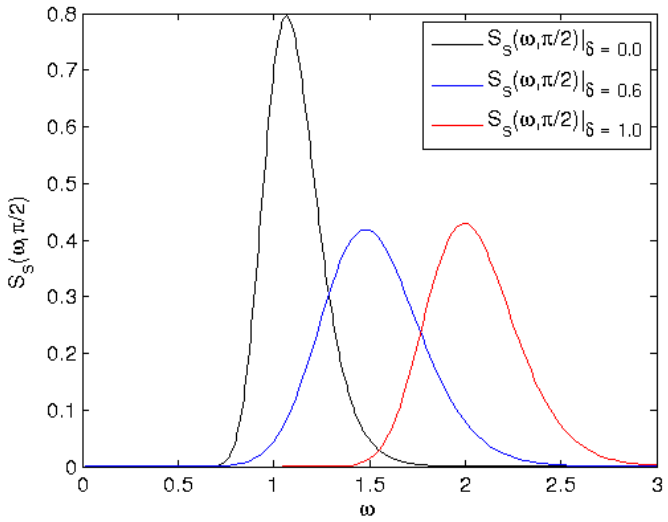

Figure C.2: Spectral function evaluated from the S^zS^z correlation, $J_{xy} = -1$, $J_z = 0$

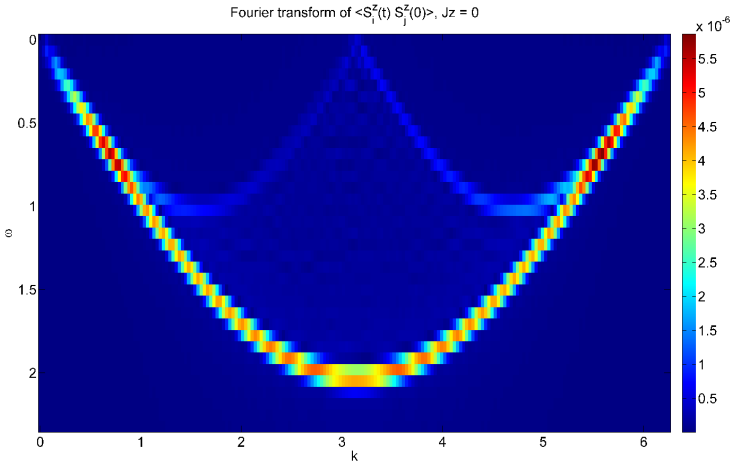

Figure C.3: Spectral function evaluated from the S^zS^z correlation by TMRG: $J_{xy} = -1, J_z = 0, L = 200, \beta = 32$ (taken from E. Rabel [42])

In Fig. C.4 we can see the behavior of the system upon increasing the static phonon displacement δ.

al. [43]

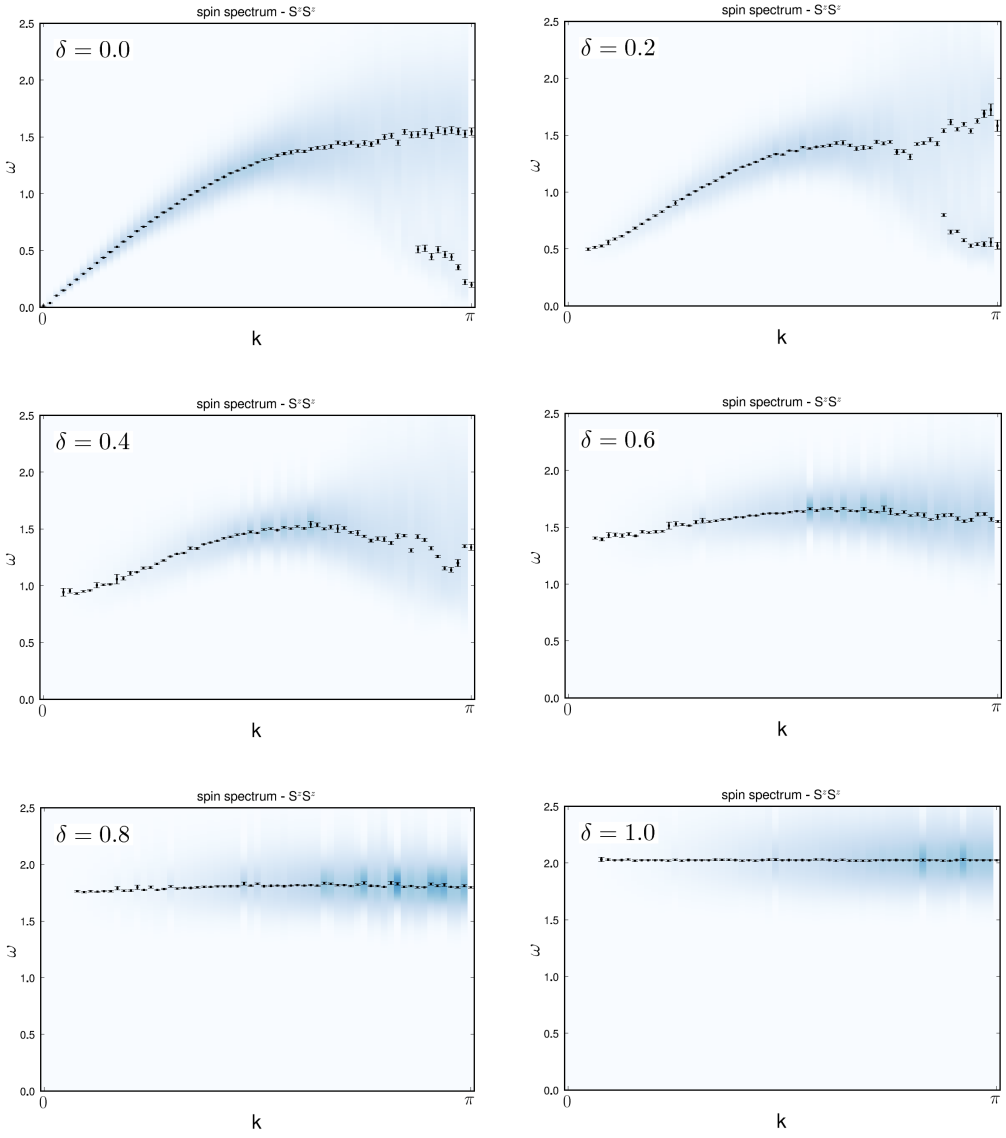

Figure C.4: Shade plots of the spin S^zS^z spectral functions: $J_{xy} = -1$, $J_z = 0, L = 128, \beta = 32$

Appendix D

Computational benchmark of the QMC- Program with dynamic Phonon Interaction

In Fig. D.1 the main structure of the QMC- program with dynamic phonon interaction is shown and the running times are analyzed with the freeware python program 'gprof2dot.py'. For simplicity edges and nodes with little impact on computation time are excluded in the flowchart. The nodes in the graph are shown as boxes, with the called function name. The total time is shown as a percentage of the total computation time and the number of function calls[1]. The most computational cost (as already mentioned) is caused by the phonon update ('do_update'-function call of the 'PhononsInX'-class), whereas the diagonal update and the worm update needs only a small percentage of the whole update time.

[1] A small two-dimensional system with $L = 8$, $W = 8$, $g = 0.3$, $J = -1$, $\beta = 10$ and 10000 sweeps was tested as an example.

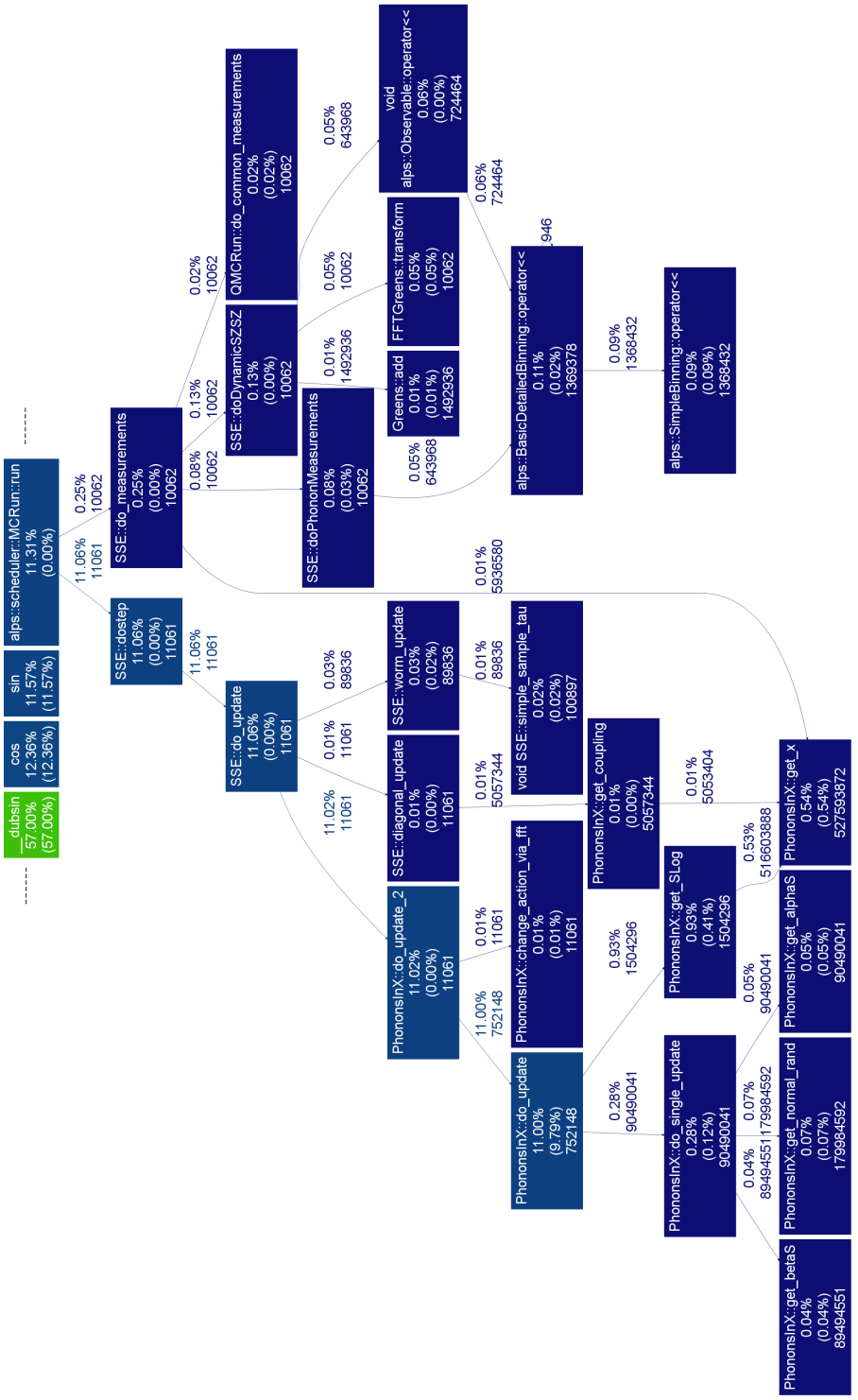

Figure D.1: Benchmark of the QMC- program with dynamic phonon interaction, analyzed with 'gprof2dot.py' excluding edges and nodes with little impact on the total computation time

Bibliography

[1] Peierls, Sir Rudolf E.: *Quantum theory of solids*. 5. Oxford University Press, 2001. – 248 S

[2] Michel, Franz: *Phonon Spectra at Quantum Phase Transitions of Spin-Peierls Systems*. itp.tugraz.at. Dissertation TU Graz, 2006

[3] Michel, Franz ; Evertz, Hans-Gerd: Lattice dynamics of the Heisenberg chain coupled to finite frequency bond phonons. In: *arXiv: 0705.0799* (2007)

[4] Sirker, Jesko ; Herzog, Alexander ; Oles, Andrzej ; Horsch, Peter: Thermally Activated Peierls Dimerization in Ferromagnetic Spin Chains. In: *Physical Review Letters* 101 (2008), Nr. 15

[5] Stuttgart, Universität: View along the stack of $(TMTSF)_2PF_6$. In: *www.pi1.uni-stuttgart.de/research/Elektronen/TMTSF_e.php* (2010)

[6] Bethe, H.: Zur Theorie der Metalle. In: *Zeitschrift für Physik A Hadrons and Nuclei* 71 (1931), S. 205–226

[7] Faddeev, L. D. ; Takhtajan, L. A.: What is the spin of a spin wave? In: *Physics Letters A* 85 (1981), Nr. 6-7, S. 375 – 377

[8] Klümper, A. ; Johnston, D. C.: Thermodynamics of the Spin- 1/2 Antiferromagnetic Uniform Heisenberg Chain. In: *Phys. Rev. Lett.* 84 (2000), Nr. 20, S. 4701–4704

[9] Mermin, N. D. ; Wagner, H.: Absence of Ferromagnetism or Antiferromagnetism in One- or Two-Dimensional Isotropic Heisenberg Models. In: *Physical Review Letters* 17 (1966), Nr. 22, S. 1133

[10] Czycholl, Gerd: Theoretische Festkörperphysik. In: *Springer Berlin Heidelberg* (2008), S. 39–92

[11] Radtke, G. ; Saùl, A. ; Dabkowska, H. A. ; Gaulin, B. D. ; Botton, G. A.: Electronic structure of the quasi-two-dimensional spin-gap system SrCu_2(BO_3)_2 : Experiment and theory. In: *Physical Review B* 77 (2008), Nr. 12, S. 125130

[12] Ding, Hong-Qiang ; Makivić, Miloje S.: Spin correlations of 2D quantum antiferromagnet at low temperatures and a direct comparison with neutron-scattering experiments. In: *Phys. Rev. Lett.* 64 (1990), Nr. 12, S. 1449–1452

[13] Sirker, J. ; Klümper, A. ; Hamacher, K.: Ground-state properties of two-dimensional dimerized Heisenberg models. In: *Physical Review B* 65 (2002), Nr. 13

[14] Wenzel, Sandro ; Bogacz, Leszek ; Janke, Wolfhard: Evidence for an Unconventional Universality Class from a Two-Dimensional Dimerized Quantum Heisenberg Model. In: *Physical Review Letters* 101 (2008), Nr. 12, S. 127202

[15] von der Linden, W.: Numerical treatment of Many-Body Problems. In: *Lecture Notes, itp.tugraz.at* (2009)

[16] Suzuki, Masuo: Relationship between d-Dimensional Quantal Spin Systems and (d+1)-Dimensional Ising Systems: Equivalence, Critical Exponents and Systematic Approximants of the Partition Function and Spin Correlations. In: *Progress of Theoretical Physics* 56 (1976), Nr. 5, S. 1454–1469

[17] Trotter, H. F.: On the product of semi-groups of operators. In: *Proc. Amer. Math. Soc.* 10 (1959), S. 545–551

[18] Evertz, H. G.: The Loop Algorithm. In: *Advances in Physics* (2003)

[19] Sandvik, A. ; Singh, R. ; Campbell, D.: Quantum Monte Carlo in the interaction representation: Application to a spin-Peierls model. In: *Physical Review B* 56 (1997), Nr. 22, S. 14510–14528

[20] Alet, F. ; Dayal, P. ; Grzesik, A. ; Honecker, A. ; Koerner, M. ; Laeuchli, A. ; Manmana, S. R. ; McCulloch, I. P. ; Michel, F. ; Noack, R. M. ; Schmid, G. ; Schollwoeck, U. ; Stoeckli, F. ; Todo, S. ; Trebst, S. ; Troyer, M. ; Werner, P. ; Wessel, S. ; the ALPS collaboration: The ALPS project: Open source software for strongly correlated systems. In: *cond-mat/0410407* (2004). – J. Phys. Soc. Jpn. Suppl. 74 (2005) 30

[21] Henelius, Patrik ; Sandvik, Anders: Sign problem in Monte Carlo simulations of frustrated quantum spin systems. In: *Physical Review B* 62 (2000), Nr. 2, S. 1102–1113

[22] Syljuåsen, Olav F. ; Sandvik, Anders W.: Quantum Monte Carlo with directed loops. In: *Phys. Rev. E* 66 (2002), Nr. 4, S. 046701

[23] Prokof'ev, N. V. ; Svistunov, B. V. ; Tupitsyn, I. S.: Exact, Complete, and Universal Continuous-Time Worldline Monte Carlo Approach to the Statistics of Discrete Quantum Systems. In: *cond-mat/9703200* (1997). – Sov. Phys. - JETP 87, p. 310 (1998)

[24] Nolting, W.: *Grundkurs Theoretische Physik 7*. Bd. 6. 7. Springer, 2005. – 395–425 S

[25] Prokofév, N. V. ; Svistunov, B.V. ; Tupitsyn, I.S.: Exact quantum Monte Carlo process for the statistics of discrete systems. In: *Journal of Experimental and Theoretical Physics Letters* 64 (1996), Nr. 12, S. 911–916

[26] B. Chapman, R. Van Der P.: *Using OpenMP: Portable Shared Memory Parallel Programming*. 2. The MIT Press, 2007

[27] H.G. Evertz, W. von der L.: *Computer Simulations*. itp.tugraz.at. Lecture notes TU Graz, 2007

[28] von der Linden, W. ; Preuss, R. ; Hanke, W.: Consistent Application of Maximum Entropy to Quantum-Monte-Carlo Data. In: *cond-mat/9503098* (1995)

[29] Silver, R. N. ; Sivia, D. S. ; Gubernatis, J. E.: Maximum-entropy method for analytic continuation of quantum Monte Carlo data. In: *Physical Review B* 41 (1990), Nr. 4, S. 2380

[30] Cross, M. ; Fisher, Daniel: A new theory of the spin-Peierls transition with special relevance to the experiments on TTFCuBDT. In: *Physical Review B* 19 (1979), Nr. 1, S. 402–419

[31] Giamarchi, T.: *Quantum Physics in One Dimension*. 1. Oxford University Press, 2004

[32] Sandvik, Anders ; Campbell, David: Spin-Peierls Transition in the Heisenberg Chain with Finite-Frequency Phonons. In: *Physical Review Letters* 83 (1999), Nr. 1, S. 195–198

[33] Dorneich, Ansgar ; Troyer, Matthias: Accessing the dynamics of large many-particle systems using the stochastic series expansion. In: *Phys. Rev. E* 64 (2001), Nr. 6, S. 066701

[34] Okamoto, Kiyomi ; Nomura, Kiyohide: Fluid-dimer critical point in S = antiferromagnetic Heisenberg chain with next nearest neighbor interactions. In: *Physics Letters A* 169 (1992), Nr. 6, S. 433–437

[35] Marinari, E. ; Parisi, G.: Simulated Tempering: A New Monte Carlo Scheme. In: *EPL (Europhysics Letters)* 19 (1992), Nr. 6, S. 451

[36] Sirker, J. ; Klümper, A. ; Hamacher, K.: Ground-state properties of two-dimensional dimerized Heisenberg models. In: *Phys. Rev. B* 65 (2002), Nr. 13, S. 134409

[37] Uhrig, Götz S.: Symmetry and Dimension of the Magnon Dispersion of Inorganic Spin-Peierls Systems. In: *Phys. Rev. Lett.* 79 (1997), Nr. 1, S. 163–166

[38] Campostrini, Massimo ; Hasenbusch, Martin ; Pelissetto, Andrea ; Rossi, Paolo ; Vicari, Ettore: Critical exponents and equation of state of the three-dimensional Heisenberg universality class. In: *Phys. Rev. B* 65 (2002), Nr. 14, S. 144520

[39] Favorsky, I A. ; Kuznetsova, T V. ; Vorontsov-Velyaminov, P N.: Numerical simulations of quantum two-dimensional Heisenberg ferromagnetics. In: *Journal of Physics: Condensed Matter* 4 (1992), Nr. 10, S. 2629

[40] Sengupta, P.: Neel to spin-Peierls transition in the ground state of a quasi-1D Heisenberg model coupled to bond phonons. In: *arXiv:cond-mat/0307746* (2003)

[41] Okamoto, Kiyomi ; Sugiyama, Tadao: Ground-State of Spin-1/2 Alternating Heisenberg-XY Ferromagnet in One Dimension. In: *Journal of the Physical Society of Japan* 57 (1988), S. 1610–1620

[42] Rabel, E.: *Quantum Physics in One Dimension.* itp.tugraz.at. TU Graz, 2010

[43] Gouvêa, M. E. ; Pires, A. S. T.: One-dimensional XY antiferromagnetic Heisenberg model with nearest and next nearest neighbour exchange interactions. In: *Physica Status Solidi (b)* 242 (2005), Nr. 12, S. 2530–2539

Acknowledgment

First of all I would like to thank my parents who supported me and helped me to make this study possible, precisely because it is very often taken for granted. Thanks to my sister, my friends and colleagues for spending a nice time off with them, recharging my batteries.

At this point, I would also like to thank Professor Hans-Gerd Evertz for guiding me through this thesis, for intensive joint discussions and his open door at any time. Special thanks to Peter Pippan, Ralf Gamillscheg and the members of my office Elias Rabel, Martin Ganahl and Valentin Zauner. These colleagues were always willing to answer yet another small question. I also want to mention Andreas Hirczy our administrator of the institute and thus a central point of contact - special thanks to him and his suggestions. Furthermore I want to thank all members of the 'Condensed Matter Physics group', for access to their work, methods and solutions.

Finally I want to thank Frank Messner, Alexander Schmon and Xiang Zhou for hundreds of coffee brakes, with more or the less physical discussions.